Critical importance of DNA binding for CSL protein functions in fission yeast

Anna Marešová[1], Martina Oravcová[1], María Rodríguez-López[4], Miluše Hradilová[2], Viacheslav Zemlianski[1], Robert Häsler[3], Pablo Hernández[4], Jürg Bähler[5], Martin Převorovský[1,*]

[1]Department of Cell Biology, Faculty of Science, Charles University, Viničná 7, 128 00 Prague 2, Czechia
[2]Laboratory of Genomics and Bioinformatics, Institute of Molecular Genetics of the Czech Academy of Sciences, Vídeňská 1083, 142 20 Prague 4, Czechia
[3]Center for Inflammatory Skin Diseases, Department of Dermatology and Allergy, University Hospital Schleswig-Holstein, Campus Kiel, Rosalind-Franklin-Straße 9, 24105 Kiel, Germany
[4]Department of Cellular and Molecular Biology, Centro de Investigaciones Biológicas Margarita Salas, Consejo Superior de Investigaciones Científicas, Ramiro de Maeztu 9, 28040 Madrid, Spain
[5]Institute of Healthy Ageing and Department of Genetics, Evolution & Environment, University College London, Gower Street, London WC1E 6BT, UK

* corresponding author; prevorov@natur.cuni.cz

Keywords: CSL proteins, fission yeast, DNA binding, lipid metabolism, chromatin structure, cell adhesion, genome integrity

SUMMARY STATEMENT

CSL transcription factors regulate a diverse set of processes, but the mechanisms are not always clear. We show that *S. pombe* CSL proteins need the ability to bind DNA for most of their roles.

ABSTRACT

CSL (CBF1/RBP-Jκ/Suppressor of Hairless/LAG-1) proteins are conserved transcription factors found in animals and fungi. In fission yeast, they regulate various cellular processes, including cell cycle progression, lipid metabolism, and cell adhesion. CSL proteins bind to DNA through their N-terminal Rel-like domain and central beta-trefoil domain. Here, we investigated the importance of DNA binding for CSL functions in the fission yeast *Schizosaccharomyces pombe*. We created CSL mutants with disrupted DNA binding and found that the vast majority of CSL functions depend on intact DNA binding. Specifically, DNA binding is crucial for the regulation of cell adhesion, lipid metabolism, cell cycle progression, long non-coding RNA expression, and genome integrity maintenance. Interestingly,

perturbed lipid metabolism leads to chromatin structure changes, potentially linking lipid metabolism to the diverse CSL-associated phenotypes. Our study highlights the critical role of DNA binding for CSL protein functions in fission yeast.

INTRODUCTION

CSL (CBF1/RBP-Jκ/Suppressor of Hairless/LAG-1) proteins, a structurally unique and conserved family of transcription factors, are found in animals and fungi (with the exception of most Ascomycetes) (Hall and Kovall, 2019; Převorovský et al., 2007). Their regulatory roles in animal development have been studied extensively (for a review, see e.g. (Borggrefe and Oswald, 2009)), while the fungal CSL proteins have only been characterized in the fission yeast *Schizosaccharomyces pombe*, where they regulate cell cycle progression, lipid metabolism, and cell adhesion (Kwon et al., 2012; Převorovský et al., 2009; Převorovský et al., 2015; Vachon et al., 2013). The mechanism of CSL protein binding to DNA has been characterized in detail, and is mediated by the N-terminal Rel-like domain (NTD) together with the central beta-trefoil domain (BTD) (Kovall and Hendrickson, 2004). Notably, the DNA binding mode seems to be conserved over a large evolutionary distance, as BTD mutations disrupting DNA binding in the murine RBP-Jκ protein (substitution R218H; (Chung et al., 1994)) also abolish binding to DNA of fission yeast Cbf11 (substitution R318H) and Cbf12 (substitution R644H) CSL paralogs (Oravcová et al., 2013).

CSL proteins were shown to participate in numerous processes in *S. pombe*, with Cbf11 often acting as an antagonist of Cbf12 (Převorovský et al., 2009). For example, Cbf12 is required for cell-surface and cell-cell adhesion (non-sexual flocculation). Cells lacking Cbf12 lose their ability to adhere, while overexpression of Cbf12 leads to a hyper-adhesive phenotype. On the contrary, cells lacking Cbf11 show increased adhesion, and adhesion is abolished upon overexpression of Cbf11 (Kwon et al., 2012; Převorovský et al., 2009). Later, it was shown that CSL proteins are part of an elaborate network of several transcription factors which regulate flocculation by activating or repressing genes encoding adhesive cell-surface proteins (flocculins *gsf2*, *pfl2-pfl9*; (Kwon et al., 2012; Linder and Gustafsson, 2008)) and cell wall-remodeling enzymes (Kwon et al., 2012). Cbf12 is upregulated in the stationary phase of growth (Převorovský et al., 2009), when cell adhesion naturally increases, and Cbf12 can activate its own transcription in a positive feedback loop (Kwon et al., 2012).

Likewise, the transcriptional regulation of lipid metabolism genes in *S. pombe* is controlled by a network of at least three transcription factors. The metabolism of triglycerides is controlled by the transcription factors Cbf11 and Mga2, which share some target genes (Burr et al., 2016; Převorovský et al., 2015; Převorovský et al., 2016). On the other hand, the metabolism of sterols is controlled by Sre1 (mammalian SREBP-2 homolog), and there is crosstalk between Sre1 and Mga2 that coordinates the two branches of lipid metabolism (Burr et al., 2016; Burr et al., 2017). Intriguingly, *S. pombe* contains another SREBP paralog, Sre2, which does not seem to regulate lipid metabolism, but is involved in regulating flocculation (Kwon et al., 2012). This is reminiscent of the relationship

between the Cbf11 and Cbf12 CSL paralogs (Převorovský et al., 2009). The target genes of Cbf11 include the *cut6* acetyl-coenzyme A carboxylase (the rate-limiting enzyme of fatty acid synthesis), *ole1* acyl-coenzyme A desaturase, long-chain fatty acid-coenzyme A ligases *lcf1* and *lcf2*, and *bio2* biotin synthase and *vht1* biotin transporter (biotin is a cofactor for Cut6) (Převorovský et al., 2015). Cells lacking *cbf11* or overexpressing *cbf12* also display a range of defects related to cell cycle progression (Převorovský et al., 2009). Most notably, CSL manipulations lead to increased incidence of a particular form of catastrophic mitosis ("cut" phenotype; (Převorovský et al., 2009; Yanagida, 1998)), a phenotype shared with several other lipid-related mutants (Zach and Převorovský, 2018). It was suggested that, when fatty acid production is inhibited, there is insufficient supply of phospholipids for nuclear envelope expansion during the anaphase of the closed mitosis in *S. pombe*, and this results in spindle collapse and mitotic failure (Makarova et al., 2016; Takemoto et al., 2016). Moreover, we recently identified additional factors contributing to mitotic defects in *Δcbf11* cells, such as perturbed structure of centromeric chromatin and aberrant cohesin occupancy (Vishwanatha et al., 2023). However, the molecular details of how dysregulated lipid metabolism leads to these various cell cycle defects remain elusive. Interestingly, lipid metabolism has a pronounced impact on chromatin structure and proper regulation of stress gene expression. For example, cells expressing the Cbf11DBM mutant protein with abolished DNA binding (the above-mentioned R318H substitution) show wide-spread changes in histone H3 lysine 9 (H3K9) modifications, including specific H3K9 hyperacetylation and derepression of oxidative stress response genes, which is mediated by the histone acetyltransferases Gcn5 and Mst1 (Princová et al., 2023).

Transcription regulators can control their target genes by binding DNA either directly, or indirectly as part of a protein complex. There are also examples of transcription factors with moonlighting roles, completely independent of their transcription factor functions (Lee et al., 2003; Wegrzyn et al., 2009). Furthermore, mutated mammalian CSL proteins unable to bind DNA have been shown to affect signaling and gene expression by sequestering transcriptional coregulators away from DNA (Gagliani et al., 2022; Kato et al., 1997). To better understand the functional relationships within the broad spectrum of seemingly disparate roles of CSL proteins in *S. pombe*, we set out to determine the requirements for DNA binding for each known CSL role. In this study we show that the vast majority of CSL functions in *S. pombe* cells depend on their intact DNA binding domain (BTD domain). We also hypothesize that changes in chromatin structure resulting from perturbed lipid metabolism could be the unifying theme behind the diversity of CSL-associated phenotypes. Finally, we describe a novel role for CSL proteins in the maintenance of genome integrity.

RESULTS

Creation of CSL DNA binding mutant strains

To determine the importance of DNA binding activity for the various roles of fission yeast CSL proteins we employed previously described point mutations that disrupt DNA binding (DNA-binding mutation, DBM, (Oravcová et al., 2013)). We re-created the DBM mutations directly in the endogenous *cbf11*

and *cbf12* loci, respectively, and added a C-terminal TAP-tag to facilitate protein detection and purification. To introduce as few confounding factors as possible, the whole construction was performed in a scarless manner (see Materials and Methods for details), leaving no selection markers and keeping the regulatory untranslated regions intact (Wells et al., 2012). As controls, we also created TAP-tagged alleles of non-mutated *cbf11* and *cbf12* in an analogous manner. The introduction of the TAP tag did not affect growth rate. Notably, the growth of the DBM mutant strains was comparable to growth of the respective deletion mutants (Fig. S1).

DNA-binding activities of CSL proteins are required for their antagonism in cell adhesion

Cbf11 and Cbf12 antagonistically regulate adhesion to agar and cell flocculation (Převorovský et al., 2009), with Cbf12 directly activating the expression of several adhesion-related genes, including the *cbf12* gene itself (Kwon et al., 2012). When overexpressed, Cbf12 was shown to bind to the promoters of the *gsf2* and *pfl7* flocculin genes, coinciding with a marked increase in the corresponding transcript levels (Kwon et al., 2012). Moreover, Gsf2 was demonstrated to be critical for the CSL-related increased cell adhesion (Kwon et al., 2012). Notably, *cbf11DBM-TAP* cells displayed increased adhesion to agar comparable to the *Δcbf11* strain (Fig. 1A), while the adhesion of *cbf12DBM-TAP* cells was abolished as in the *Δcbf12* strain (Fig. 1B). These results indicate that the DNA binding activity is required for both CSL proteins to exert their regulatory functions in cell adhesion.

To study the effect of DBM mutations in more detail, we first performed a genome-wide ChIP-nexus analysis of CSL binding to DNA. The results showed a global decrease in Cbf12DBM-TAP binding to its known target loci, however, the ability of Cbf12DBM-TAP to bind DNA was not fully abolished *in vivo* (Fig. S2A). This is in contrast to the previous *in-vitro* studies of plasmid-expressed HA-Cbf12, where binding to DNA was no longer detectable upon the introduction of the DBM mutation (Oravcová et al., 2013). We visually inspected ChIP-nexus read coverage at the known adhesion-related genes and identified *cbf12* and flocculins *gsf2*, *pfl7* and *pfl2* as potential targets of Cbf12 (Fig. 1D, Fig. S2B). Notably, little to no Cbf11 binding was observed at these promoters (Fig. 1D, Fig. S2B), making direct competition between Cbf11 and Cbf12 unlikely. Furthermore, of these four loci, only *pfl7* and *pfl2* showed markedly decreased CSL binding in the *cbf12DBM-TAP* mutant (Fig. 1D, Fig. S2B). Subsequent ChIP-qPCR and RT-qPCR analyses aimed at the *cbf12*, *gsf2* and *pfl7* genes confirmed the ChIP-nexus results (Fig. 1E) and showed that only the expression of *pfl7*, but not of *cbf12* and *gsf2*, was decreased in the adhesion-deficient *cbf12DBM-TAP* mutant (Fig. 1C). A similar expression pattern was observed in the *Δcbf12* strain (Fig. 1C). On the other hand, we found a different flocculin expression pattern in the hyper-adhesive *Δcbf11* and *cbf11DBM-TAP* cells, where *pfl2* and *pfl7* genes were downregulated, while *gsf2* was upregulated (Fig. S2C). Therefore, the CSL interplay in cell adhesion (and likely also the mechanism of *cbf12* autoregulation) is not straightforward, and may possibly be influenced by factors such as culture growth phase (Převorovský et al., 2009), or growth media composition (Kwon et al., 2012).

Interestingly, it was shown previously that *cbf12* mRNA level is increased 1.8-fold in *Δcbf11* cells (Kwon et al., 2012), and we found *cbf12* to be 1.3 and 1.9-fold upregulated in *Δcbf11* and *cbf11DBM-TAP* cells, respectively (Fig. S2C). Cbf11 may thus, likely indirectly, repress *cbf12*. Intriguingly, the *cbf12* transcript stability is negatively regulated by the Zfs1 RNA-binding protein (Wells et al., 2012), positioning Zfs1 as a potential intermediary between Cbf11 and Cbf12. However, we did not see any Cbf11 binding to the *zfs1* promoter, and *zfs1* expression was not affected by either *cbf11* deletion or overexpression (Převorovský et al., 2015). In any case, the ability to bind DNA is critical for CSL proteins to regulate cell adhesion.

Cbf11DBM cells recapitulate the mitotic and cellular morphology defects of *Δcbf11* cells

Cells lacking Cbf11 display defects in cell morphology (misshapen, enlarged, branched cells), septation defects (multiple septa, thick septa, filamentous growth), and are prone to catastrophic mitosis (such as “cut” phenotype) (Převorovský et al., 2009) (Fig. 2). To assess the impact of the DBM mutation on the role of Cbf11 in cell cycle regulation, we performed microscopy of WT, *cbf11-TAP*, *Δcbf11* and *cbf11DBM-TAP* cells. While the *cbf11-TAP* cells resembled WT cells, the *cbf11DBM-TAP* mutant largely recapitulated the defects of *Δcbf11* cells. Namely, the *cbf11DBM-TAP* strain showed enlarged and misshapen cells, short multicellular filaments, decondensed and/or fragmented nuclei (Fig. 2A), and increased incidence of catastrophic mitosis (Fig. 2A, B).

The *Δcbf11* mutant had been found to be sensitive to the microtubule poison thiabendazole (TBZ) in a high-throughput screen (Han et al., 2010). We recently confirmed this observation, and detected aberrant chromatin structure and cohesin occupancy at the centromeres in *Δcbf11* cells (Vishwanatha et al., 2023). When we now tested the *cbf11DBM-TAP* strain, it showed TBZ sensitivity comparable to the *Δcbf11* mutant (Fig. S3). So in summary, the DNA binding activity is critical for Cbf11 to exert its role in the regulation of cell cycle progression, mitosis and nuclear integrity.

Intact DNA-binding domain is necessary for Cbf11 to regulate lipid metabolism

Cbf11 activates the expression of several lipid metabolism genes and is required for the formation of storage lipid droplets (LDs) (Převorovský et al., 2015; Převorovský et al., 2016). We therefore tested the requirement for DNA binding of Cbf11 to exert its regulatory function in lipid metabolism. Indeed, introduction of the DBM mutation into the *cbf11* gene resulted in dysregulation of lipid metabolism very similar to that of the *Δcbf11* strain. Namely, the *cbf11DBM-TAP* culture showed pronounced cell-to-cell heterogeneity in the content of lipid droplets (Fig. 3A) and, on average, cells contained fewer and smaller LDs compared to WT (Fig. 3B). Next, we determined the expression levels of putative Cbf11 target genes involved in lipid metabolism (*cut6*, *ole1*, *lcf1*, *lcf2*, *fsh2*, *vht1*, *bio2*, *fas2*) (Převorovský et al., 2015) by RT-qPCR. With the exception of *fas2* (alpha subunit of the fatty acid synthase complex), all tested genes were significantly downregulated in *cbf11DBM-TAP* cells to a level similar to the *Δcbf11* mutant (Fig. 3C).

We then extended the analyses and quantified gene expression globally by RNA-seq of WT, *Δcbf11* and *cbf11DBM-TAP* cells. The RNA-seq results were in good agreement with our previous microarray analyses of the *Δcbf11* transcriptome (Fig. S4), and confirmed the ~50% downregulation of lipid metabolism genes in the *cbf11DBM-TAP* strain (Fig. 3D, Fig. S2D). Furthermore, there was a strong overlap in the groups of genes expressed differentially in either *Δcbf11* or *cbf11DBM-TAP* cells (Fig. 3E). Finally, ChIP-nexus and/or ChIP-qPCR analyses revealed that the decrease in gene expression in *cbf11DBM-TAP* cells coincided with loss of Cbf11DBM binding to the promoters of *cut6*, *ole1*, *lcf1* (Fig. 3F, G), and *lcf2*, *fsh2* and *ptl1* genes (Fig. S2E). Interestingly, judging by the ChIP-nexus footprints, Cbf11 seems to bind only 1 site per promoter (Fig. 3F, Fig. S2E). Taken together, the regulatory role of Cbf11 in lipid metabolism requires its ability to bind DNA, and our results confirm Cbf11 as a direct activator of gene expression.

CSL proteins are required for maintenance of genome integrity

The observations of fragmented and/or decondensed nuclei in *Δcbf11* and *cbf11DBM-TAP* cells (Fig. 2A), together with a previous report showing a requirement for the mammalian CSL/RBP-Jκ protein in the maintenance of genome integrity (Bottoni et al., 2019), prompted us to test the sensitivity of CSL mutants to genotoxic stress. Indeed, when exposed to camptothecin (CPT), a topoisomerase I inhibitor causing double-stranded DNA breaks, the *Δcbf11* cells showed clear sensitivity to the drug (Fig. 4A). Surprisingly, the *Δcbf12* strain was also sensitive to CPT, albeit to a lesser extent (Fig. 4A). To our knowledge, this is the first case where the effects of manipulating the respective CSL paralogs are not antagonistic. Notably, the *Δcbf11 Δcbf12* double mutant showed CPT sensitivity comparable to the *Δcbf11* strain (Fig. 4A). The absence of any clear additive effects on CPT sensitivity in the double mutant suggests that both CSL paralogs affect the same process or pathway. Thus, our genetic analyses indicate that Cbf11 is more important for the maintenance of genome integrity than Cbf12, and that Cbf11 likely acts downstream of Cbf12.

Next, we tested the impact of CSL DBM mutations on the cellular resistance to genotoxic stress. While the *cbf11DBM-TAP* cells showed CPT sensitivity comparable to *Δcbf11*, the *cbf12DBM-TAP* mutant strain was not sensitive to CPT, in stark contrast to the *Δcbf12* cells (Fig. 4B). Thus, the DNA binding activity of Cbf12 may not be required for its role in the maintenance of genome integrity, and *cbf12DBM-TAP* may be a separation-of-function mutation. Alternatively, the residual DNA-binding activity of Cbf12DBM (Fig. S2A) may be sufficient to support its function in the maintenance of genome integrity and no mutant phenotype is manifested in this case.

We recently showed that mutations in *cbf11* and several lipid metabolism genes (including *cut6*) result in widespread changes in chromatin structure and in altered expression of oxidative stress-response genes (Princová et al., 2023; Vishwanatha et al., 2023). Therefore, we tested whether there is a more general link between lipid metabolism and the cellular resistance to genotoxic stress. Interestingly, the *Pcut6MUT* mutant, which lacks the Cbf11 binding site in the *cut6* promoter and displays ~50% reduction in *cut6* expression (Převorovský et al., 2016), was also sensitive to CPT (Fig. 4C). This result suggests that unperturbed fatty acid synthesis is indeed important for the cell's ability to resist

genotoxic stress caused by CPT. Moreover, when we overexpressed *cut6* in the *Δcbf11* background, compensating the reduced *cut6* expression in cells lacking Cbf11, the *Δcbf11* sensitivity to CPT was partially rescued (Fig. 4C). Therefore, the Cbf11-mediated transcriptional regulation of lipid metabolism is required for the maintenance of genome integrity.

To determine the specificity of the observed phenomenon, we treated CSL mutants with methyl methanesulfonate (MMS) or hydroxyurea (HU). MMS causes DNA damage by alkylation, while HU causes various DNA lesions by inhibiting DNA replication (Noguchi et al., 2009). As shown in Fig. 4D, the sensitivity of *Δcbf11* and *Δcbf12* cells to MMS was comparable to WT. Cells lacking *cbf12* showed increased sensitivity to HU, while *Δcbf11* cells were strongly resistant to HU. This latter finding may be explained by the increased reductive capacity of *Δcbf11* cells (Princová et al., 2023), as the effects of HU are redox-dependent (Singh and Xu, 2016). Taken together, the sensitivity of CSL mutants to genotoxic stress seems to be limited to specific sources and/or types of DNA damage.

Non-coding RNAs are upregulated in cells lacking intact DNA binding domain of Cbf11

Global perturbations of chromatin structure can result in aberrant expression of various non-coding RNAs (Anderson et al., 2009; Atkinson et al., 2018). Therefore, we used RNA-seq to characterize the non-coding transcriptomes of cells lacking intact Cbf11. As previously reported (Marguerat et al., 2012), on average, the expression of long non-coding RNAs (lncRNAs) is markedly lower compared to coding genes (Fig. 5A). Many annotated lncRNAs might be a mere result of transcriptional noise(Atkinson et al., 2018), while others have cellular functions in specific environmental or physiological contexts (Rodriguez-Lopez et al., 2022). Interestingly, hundreds of lncRNAs showed significant changes in expression in both *Δcbf11* and *cbf11DBM-TAP* cells compared to WT, with both the number and amplitude of expression changes being larger in the direction of upregulation (Fig. 5A; 1568 up- and 656 downregulated in *Δcbf11*; 1011 up- and 363 downregulated in *cbf11DBM-TAP*). Intriguingly, the changes in lncRNA expression correlated well with the degree of histone H3 lysine 9 acetylation (H3K9ac) at the respective lncRNA loci in the *Δcbf11* mutant (Fig. 5B). Therefore, we conclude that the DNA binding activity of Cbf11 is also required for proper expression of the non-coding transcriptome.

Cells lacking Cbf11 show aberrant cell cycle arrest in response to CPT

CPT treatment causes double-stranded DNA breaks in DNA and triggers the DNA damage checkpoint. This arrests cell cycle progression to give cells time to repair the damage (Noguchi et al., 2009; Wan et al., 1999). To gain more insight into the CPT sensitivity of CSL mutants we next analyzed DNA damage checkpoint functionality in these strains. In contrast to the chronic CPT exposure on plates (Fig. 4A), when exposed to an acute dose of 40 µM CPT for up to 6 hours, the *Δcbf11* and *Δcbf12* mutants did not show CPT hypersensitivity. As a control, we used cells lacking the general DNA checkpoint kinase Rad3/ATR, which were killed by CPT within 2 hours (Fig. 4E). Rad3 phosphorylates and activates the Chk1 DNA damage checkpoint kinase, which can be observed as

retarded migration of Chk1 in a polyacrylamide gel (Noguchi et al., 2009; Wan et al., 1999). Chk1 phosphorylation in response to CPT appeared normal in both *Δcbf11* and *Δcbf12* cells (Fig. 4F).

The DNA damage checkpoint blocks cell cycle progression, but does not inhibit cell growth. As a result, there is a drop in the number of dividing cells in the population, and the cells become elongated (Noguchi et al., 2009). Notably, the number of binucleate (i.e., dividing) cells did not decrease in *Δcbf11* and *Δcbf11 Δcbf12* cultures treated with CPT (Fig. 4G), and the cells did not elongate as much as WT cells did (Fig. 4H), indicative of ongoing cell division. This was likely not due to a general problem with cell cycle arrest, as *Δcbf11* arrested and elongated normally when blocked at G2/M by the inactivation of Cdc25 (Fig. 4H). The aberrant cell cycle arrest was also apparent at the level of transcriptome. The expression of periodic genes regulated by the transcription factors Sep1 and Ace2 (Rustici et al., 2004) is inhibited following a cell cycle arrest, but this decrease in expression was delayed and/or compromised in *Δcbf11* cells treated with 20 μM CPT (Fig. 6A, B). Cdc10 regulates S-phase genes involved in DNA synthesis (Rustici et al., 2004), and these genes are also induced in response to DNA damage to facilitate repair (de Bruin et al., 2008). Intriguingly, compared to WT, Cdc10-regulated genes were hyper-induced in *Δcbf11* cells treated with CPT (Fig. 6B). We also noted that genes induced specifically by ionizing radiation (Watson et al., 2004), which also causes double-stranded DNA breaks, are upregulated both in untreated and CPT-treated *Δcbf11* cells (Fig. 6B). In summary, CPT-induced cell cycle arrest is aberrant in cells lacking Cbf11 and, even without external genotoxic stress, these cells show a transcriptional signature that suggests presence of DNA damage.

Cbf11 is required for the stability of rDNA arrays

Based on the results of our transcriptomic studies (Fig. 6), we investigated whether *Δcbf11* cells have more DNA damage. To this end, we quantified the fractions of untreated WT and *Δcbf11* nuclei that showed at least one Rad52 DNA repair focus (Noguchi et al., 2009). Indeed, we found that the fraction of nuclei with Rad52 foci was increased by 1.6-fold in the *Δcbf11* mutant (Fig. 7A). Next, we determined the subnuclear localization of the Rad52 foci by using cells with fluorescently labeled histone H3 (Hht1-mRFP). In these cells, the spherical nucleus is clearly divided into the chromatin territory (red) and nucleolar territory (dark). Strikingly, the increase in Rad52 foci was most pronounced inside the nucleolus or at the border region between the nucleolus and chromatin (Fig. 7B).

The nucleolus is the site of ribosome biogenesis and contains ribosomal DNA (rDNA). rDNA is organized as two multi-copy tandem arrays (~100-120 copies in total) at both ends of chromosome III in fission yeast (Wood et al., 2002), and represents a fragile region prone to DNA damage (Rozenzhak et al., 2010). Strikingly, pulse-field gel electrophoresis (PFGE) analysis showed that chromosome III was markedly shorter in numerous *Δcbf11* clones (Fig. S5). Subsequent targeted analysis of rDNA size by PFGE and Southern blot of PvuII-digested chromosomes confirmed decreased rDNA copy number in *Δcbf11* cells (Fig. 7C). Also, RT-qPCR showed that rRNA transcript levels were decreased by 45% in *Δcbf11* cells (Fig. 7D).

Then we checked for any potential binding of CSL proteins to rDNA. Only several innermost rDNA copies have been assembled in the reference fission yeast genome (Wood et al., 2002). Unfortunately, the ChIP-nexus coverage in these complex regions was inconclusive. Therefore, we reanalyzed our previously published ChIP-seq data (Převorovský et al., 2015). While we did not find any binding of Cbf11 here, we found a clear Cbf12 binding site located close to the rDNA replication origin (*ars3001*; Fig. 7E). However, the functional significance of this Cbf12 binding is not clear.

Finally, rDNA array stability depends upon proper coordination of rRNA transcription with DNA replication (Kobayashi et al., 1998). To this end, several unidirectional replication fork barriers (RFBs) are present in each rDNA copy, and some of them are operated by the Reb1 or Sap1 DNA-binding proteins (Mejía-Ramírez et al., 2005; Sánchez-Gorostiaga et al., 2004). When we performed ChIP-qPCR, we found 2.5-fold increased Reb1 occupancy at rDNA in the *Δcbf11* mutant (Fig. 7F). To test whether Reb1 was implicated in the compromised genome integrity of cells lacking Cbf11, we deleted the *reb1* gene in the *Δcbf11* background. Strikingly, the *Δcbf11 Δreb1* double mutant showed improved growth rate (see colony size in Fig. 7G), and lower sensitivity to CPT and TBZ compared to the *Δcbf11* parent (Fig. 7G).

DISCUSSION

The CSL proteins have been implicated in numerous cellular processes in the fission yeast *S. pombe*. Cells lacking CSL genes display a wide range of phenotypes, including altered cell cycle progression, lipid metabolism, resistance to stresses or cell adhesion (Kwon et al., 2012; Převorovský et al., 2009; Převorovský et al., 2015; Převorovský et al., 2016; Vachon et al., 2013; Vishwanatha et al., 2023). CSL proteins are transcription factors (Oravcová et al., 2013), however, so far only two CSL-regulated processes have been directly linked to their transcription factor activities: activation of lipid metabolism genes by Cbf11 (Převorovský et al., 2016) (Fig. 3), and activation of adhesion-related genes by Cbf12 (Kwon et al., 2012) (Fig. 1). It was therefore possible that CSL proteins might have additional modes of functioning, independent of their transcription factor activity. Indeed, examples of transcription factors with DNA binding-independent moonlighting roles in other cellular processes have been reported (Lee et al., 2003; Wegrzyn et al., 2009). To shed more light on the ways in which CSL roles are carried out, we investigated the phenotypes of carefully constructed mutants with compromised DNA binding activities of Cbf11 or Cbf12. Our results show that the vast majority of known CSL functions in *S. pombe* depend on their ability to bind DNA (the only potential exception being the role of Cbf12 in resistance to genotoxic stress). Nevertheless, for many of these roles the exact mechanism(s) of regulation remains to be established.

Notably, most CSL mutant phenotypes are caused by perturbations of the *cbf11* paralog, while *cbf12* seems to be involved almost exclusively in cell adhesion. Importantly, in the present study we show that the DNA binding activity of Cbf11 is implicated in all its known functions, with the regulation of lipid metabolism genes remaining the best characterized role of Cbf11. Strikingly, we showed that

perturbed fatty acid synthesis results in large-scale changes in histone modifications (H3K9 acetylation and methylation), which also affect gene expression (Princová et al., 2023; Vishwanatha et al., 2023) (Fig. 5). The synthesis of fatty acids consumes acetyl-coenzyme A, a central metabolite that also acts as a substrate for protein acetylation. It is therefore tempting to speculate that changes in chromatin structure resulting from perturbed lipid metabolism and mediated by histone acetyltransferases (Princová et al., 2023) could be the root cause underlying the wide range of defects observed in *cbf11* mutant cells. For example, perturbed centromeric chromatin might be responsible for the altered expression of centromere-proximal genes, decreased mitotic fidelity, and sensitivity to microtubule poisons observed in ***Δcbf11*** cells (Vishwanatha et al., 2023). In line with this proposition, centromeric heterochromatin was shown to be important for proper centromere function in mitosis (Volpe et al., 2002). Next, mutations in several major fission yeast regulators of chromatin structure are known to compromise genome integrity and lead to sensitivity to genotoxic insults. These regulators include the sole *S. pombe* histone methyltransferase Clr4 and the essential Clr6 histone deacetylase (both target H3K9 and are required for heterochromatin formation), and the HIRA histone chaperone complex (Deshpande et al., 2009; Nicolas et al., 2007; Pan et al., 2012). Finally, perturbed chromatin is generally more prone to aberrant transcription (Anderson et al., 2009; Atkinson et al., 2018), which could explain the striking and widespread upregulation of lncRNA genes in the *cbf11* mutants (Fig. 5). Based on these findings, we propose that mere changes in lipid metabolism (such as decreased rate of fatty acid synthesis) may have far reaching and previously unappreciated consequences for the proper functioning of numerous, seemingly unrelated, important cellular processes.

In this work, we have also uncovered and characterized a novel CSL function in the maintenance of genome integrity. Strikingly, cells lacking Cbf11 show hallmarks of DNA damage, namely of double-stranded DNA breaks, predominantly in the nucleolus/rDNA (Figs. 6 and 7). rDNA arrays are complex, fragile loci, and cells evolved elaborate mechanisms to maintain their stability and copy number, including the unidirectional RFBs (Hori et al., 2023). rDNA represents ~10% of the fission yeast genome (Wood et al., 2002). With each rDNA repeat harboring a replication origin and several non-coding RNA transcription units, rDNA arrays can sequester proteins related to DNA transcription, replication and repair (Kobayashi, 2011). Indeed, the integrity of the rDNA arrays was found to be crucial for proper function of the DNA damage checkpoint and for the maintenance of integrity of the whole genome (Ide et al., 2010). The Reb1 protein is required for RFB function (Sánchez-Gorostiaga et al., 2004) and for higher-order chromosome organization within the nucleus (Singh et al., 2010). Intriguingly, we found increased Reb1 occupancy at rDNA in ***Δcbf11*** cells (Fig. 7). Since the deletion of the *reb1* gene largely suppressed the CPT sensitivity of ***Δcbf11*** cells, it is tempting to speculate that aberrant Reb1 function is responsible for the defects in genome integrity maintenance in this mutant, possibly by interfering with the mechanism(s) stabilizing rDNA copy number. However, further details will need to be established by future studies.

MATERIALS AND METHODS

Cultivations, media and strains

The *Schizosaccharomyces pombe* cells were grown according to standard procedures (Petersen and Russell, 2016) in complex yeast extract medium with supplements (YES) at 32°C, or 25°C (temperature-sensitive strains). Routine optical density (OD) measurements of liquid cell cultures were taken using the WPA CO 8000 Cell Density Meter (Biochrom). Cells were grown to either exponential or stationary phase according to the nature of the experiment. Regarding exponential phase, cells were allowed to reach OD_{600} 0.5. When cultivated to stationary phase, exponentially growing cells were diluted to OD_{600} 0.03-0.15 in fresh medium and cultivated for additional 21-24 hours. Growth rate measurements and calculation of cell culture doubling time (DT) were performed as described previously (Zach et al., 2018). Significance of differences in mutant doubling times was determined by a two-tailed unpaired t-test. Statistical tests were performed on raw data (DT in minutes), however, values normalized to WT were used for plotting to allow for more intelligible visualization. The list of strains used in this study is provided in Table S1.

Construction of strains

Construction of the scarless knock-in strains expressing C-terminally TAP-tagged Cbf11 or Cbf11DBM from its endogenous chromosomal locus was described previously (Princová et al., 2023).

The Cbf12-TAP scarless knock-in strain was constructed by a two-step gene tagging approach using *ura4* selection. First, to replace the 3' end of *cbf12* ORF in its chromosomal locus, an auxotrophic WT strain (PN559; *ura4-D18*, *leu1-32*, *ade6-M216*, h^-) was transformed using the standard lithium acetate method (Bähler et al., 1998) with a plasmid carrying the $ura4^+$ sequence surrounded by *cbf12* fragments used for homologous recombination (plasmid pMaP21 digested by SalI, KasI, and AlwNI). After selection on EMM+ade+leu plates, the integration of $ura4^+$ into the *cbf12* genomic locus was verified by PCR (primers MaP127+MP31+MP32). Then, the obtained MaP178 strain (*cbf12::*$ura4^+$, *ura4-D18*, *leu1-32*, *ade6-M216*, h^-) was used for a second integration step where a TAP-tag was introduced instead of the $ura4^+$ sequence. MaP178 cells were transformed with a fragment of the *cbf12-TAP* sequence (plasmid pMaP29 digested by SalI, KasI, and AlwNI) as template for homologous recombination. Transformants were selected on YES plates containing 5-fluoroorotic acid (5-FOA, 1 g/L) and the integration of the TAP-tagged fragment into the *cbf12* chromosomal locus was verified by PCR (primers MaP127+MaP117+MP32) and sequencing. Expression of the Cbf12-TAP protein in the resulting strain (MaP183; *cbf12-ctap4*, *ura4-D18*, *leu1-32*, *ade6-M216*, h^-) was verified by western blot with an anti-TAP antibody (Thermo Scientific, CAB1001). Prototrophic Cbf12-TAP strains (MP540/MP541) were then prepared by standard crossing and revalidated.

The Cbf12DBM-TAP scarless knock-in strain was constructed and validated analogously with some modifications. To introduce the DNA-binding mutation (DBM; R644H) (Oravcová et al., 2013) into the *cbf12* endogenous locus, MaP178 cells were transformed according to (Okazaki et al., 1990) with a fragment of the *cbf12DBM-TAP* sequence (plasmid pMaP25 digested by SalI and KasI) as template

for homologous recombination. Transformants were selected on PMG+ade+leu+ura+5-FOA plates. The integration of the *cbf12DBM-TAP* fragment into the *cbf12* chromosomal locus and the presence of DBM were verified by PCR (primers MaP169+MP32 and chkR+chkF, respectively) and sequencing. Verification of the Cbf12DBM-TAP protein expression in the resulting MaP187 strain (*cbf12DBM-ctap4*, *ura4-D18*, *leu1-32*, *ade6-M216*, *h*$^-$) and preparation of the final prototrophic Cbf12DBM-TAP strains (MP518/MP519) were performed as described above for Cbf12-TAP.

Other strains constructed in this study were created using standard genetic methods (Sabatinos and Forsburg, 2010).

The lists of plasmids and primers used in this study are provided in Table S2 and Table S3, respectively.

Spot tests

Exponentially growing cells were 10-fold serially diluted and spotted onto control YES plates and YES plates containing camptothecin (CPT; 4-7 µM; stock dissolved in DMSO; DMSO added to all cultures to 1% final concentration), thiabendazole (TBZ; 5 or 15 µg/mL), methyl methanesulfonate (MMS; 0.01%) or hydroxyurea (HU; 10 mM) for drug sensitivity assays. The spots were allowed to dry, plates were incubated at 32˚C and imaged on the day specified in the figure legend.

Cell survival assays

WT (JB32), *Δcbf11* (MP44), *Δcbf12* (MP21), and *Δrad3* (JB1068) cells were grown to exponential phase in YES. Cultures were treated with 40 µM CPT (with DMSO added to 1%). Culture aliquots (0.25-1.0 mL) were harvested at times 0, 1, 2, 3, 4, 5, 6 hrs, washed in 1 mL H_2O, and finally resuspended in 1 mL H_2O. Cell concentrations in each sample were measured using a Beckman Coulter Counter Z-series instrument. Sample aliquots (~500 cells in 100 µl; in triplicates) were spread on YES plates using 4 glass beads, and the number of colonies formed was determined after 5 days of incubation at 32°C. The whole experiment was performed twice.

Washing assays

Washing assays were used to study cell adhesion. Exponentially growing cells were spotted on an agar plate, incubated at 32°C for 7-8 days, and then washed carefully and evenly with a stream of water. Whole cell spots were imaged before and after washing in Fig. 1A. As for Fig. 1B, microscopic pictures of the edge of one colony were taken before and after washing.

Fluorescence microscopy

For observation of nuclear morphology, quantification of binucleate (dividing) cells, and quantification of the occurrence of the “cut” phenotype, cells were fixed in 70% ethanol, rehydrated in water, stained with 0.1-1 µg/mL DAPI and photographed using the Olympus CellR system or the Leica DM750 microscope. Frequency of “cut” phenotype occurrence was determined by manual counting of “cut”

cells using the ImageJ software, version 1.53c (Schneider et al., 2012). 200-1000 cells per sample were analyzed. To monitor cell cycle arrest following a genotoxic insult, cells were treated with 40 µM CPT (with DMSO added to 1%) for 0-8 hours prior to microscopy. Cells with the *cdc25-22* mutation were arrested at G2/M by incubation at 36°C for 4 hrs.

Analysis of lipid droplets (LDs) content and automated image processing was performed as described previously (Princová et al., 2019). Briefly, exponentially growing live cells were stained with BODIPY 493/503 (0.1 mg/mL; Invitrogen) and Cascade Blue dextran (10 mg/mL; Invitrogen) to visualize LDs and determine cell boundaries, respectively. Cells were subjected to z-stack imaging using the Olympus CellR microscope. 10-16 images per sample were then processed by an automated pipeline implemented in the MATLAB software. Resulting output data with detected cell objects and LDs were processed using R. A two-tailed unpaired t-test was used to determine statistical significance. Statistical tests were performed on raw data (dotIntensity_per_cellVolume or dots_per_cellVolume, respectively), however, values normalized to WT were used for plotting to allow for more intelligible visualization. Representative microscopic pictures of LDs were prepared by transforming z-stacked images into maximum projection and applying DIC overlay to show cell boundaries in ImageJ ver. 1.53c (Schneider et al., 2012).

To observe Rad52 foci, Rad52-YFP Hht1-mRFP (WT; MP306) and Rad52-YFP Hht1-mRFP *Δcbf11* (*Δcbf11*; MP309) cells were used for fluorescence microscopy. Exponentially growing cells were harvested and visualized using the Olympus CellR system. Images of individual nuclei were extracted using an ImageJ script. Rad52 foci occurrence was manually evaluated and nuclei were sorted to 4 categories: 1) nuclei without any Rad52 focus (“none”), 2) Rad52 focus located in the chromatin region represented by Hht1-mRFP signal (“chromatin”), 3) Rad52 focus in the nucleolus (“nucleolus”), 4) Rad52 foci at the chromatin/nucleolus border or a combination of previous categories (“border/both”). In total, 418 WT nuclei and 521 *Δcbf11* nuclei were analyzed (Fig. 7B).

RT-qPCR

Total RNA was extracted from cells at exponential (Fig. 3C, Fig. 7D) or stationary (Fig. 1C) phase using the MasterPure Yeast RNA Purification Kit including a DNase treatment step (Biosearch Technologies), and converted to cDNA using random primers and the RevertAid Reverse Transcriptase kit (Thermo Fisher Scientific) following manufacturer’s instructions. Quantitative PCR was performed in technical triplicates using the MESA GREEN qPCR MasterMix Plus for SYBR (Eurogentec) or 5x HOT FIREPol EvaGreen qPCR Supermix (Solis Biodyne) and the LightCycler 480 II instrument (Roche). For RT-qPCR normalization, *act1* (actin) (Fig. 7D) or both *act1* and *rho1* (Rho1 GTPase) (Fig. 1C, 3C) were used as internal reference genes. One (Fig. 3C) or two-sided (Fig. 1C) Mann-Whitney U test was used to determine statistical significance. All statistical tests were performed on data normalized only to internal reference genes (not to WT expression values), however, gene expression values normalized to WT were used for plotting to allow for more intelligible

visualization. At least two independent biological experiments were performed. The primers used are listed in Table S3.

ChIP-qPCR

Residual DNA binding of CSL proteins bearing the DBM mutation was measured by ChIP-qPCR. For Cbf11 ChIP-qPCR (Fig. 3G), 50 mL cultures of Cbf11-TAP/Cbf11DBM-TAP strains were grown to exponential phase and subsequently fixed with 1% formaldehyde for 30 min and quenched with 125 mM glycine. Regarding Cbf12 ChIP-qPCR (Fig. 1E), 3 mL of Cbf12/Cbf12DBM-TAP cultures at stationary phase were brought up to 50 mL with YES and immediately fixed as described above. Cells were washed with distilled water and broken with glass beads in Lysis Buffer (50 mM Hepes pH 7.6, 1 mM EDTA pH 8.0, 150 mM NaCl, 1% Triton X-100, 0.1% sodium deoxycholate, FY protease inhibitors [Serva]) using the FastPrep24 machine (MP Biomedicals). Extracted chromatin was sheared with the Bioruptor sonicator (Diagenode) using 20 cycles of 30 s on, 30 s off at high power settings. An aliquot of chromatin extract was kept as input control, and 0.5-1 mg of chromatin extract was used for overnight immunoprecipitation with 30 µl of BSA-blocked magnetic IgG-coated beads (Invitrogen, 110.41). The precipitated material was washed twice with Lysis Buffer (see above), Lysis 500 Buffer (50 mM Hepes pH 7.6, 1 mM EDTA pH 8.0, 500 mM NaCl, 1% Triton X-100, 0.1% sodium deoxycholate), LiCl/NP-40 Buffer (10 mM Tris-HCl pH 8.0, 1 mM EDTA pH 8.0, 250 mM LiCl, 1% Nonidet P-40, 1% sodium deoxycholate), once in TE (10 mM Tris-HCl pH 8.0, 1 mM EDTA), and eluted in Elution Buffer (50 mM Tris-HCl pH 8.0, 10 mM EDTA, 1% SDS). Cross-links were reversed at 65°C for 6 h, samples were treated with DNase-free RNase A followed by proteinase K digestion, and DNA was purified using standard phenol-chloroform extraction and sodium acetate/ethanol precipitation. Quantitative PCR was performed using the 5x HOT FIREPol EvaGreen qPCR Supermix (Solis Biodyne) and the LightCycler 480 II instrument (Roche) as technical triplicates. Signal (C_t values) at *act1* locus (Fig. 1E) or geometric average of signals at three loci (*act1*, *sty1*, M40) (Fig. 3G) were used as negative controls. Three independent biological replicates were performed.

ChIP-qPCR analysis of Reb1 binding to the rDNA locus shown in the main text (Fig. 7F) was performed analogously with some exceptions. Briefly, 50 mL cultures of Reb1-TAP (WT; MP380) or Reb1-TAP *Δcbf11* (*Δcbf11*; MP487, MP488) cells were used and the immunoprecipitated DNA was washed with IP buffer (50 mM Tris-HCl pH 7.5, 150 mM NaCl, 5 mM EDTA, 1% Triton X-100, 0.5% Nonidet P-40), and purified using 10% Chelex 100 resin (Bio-Rad). Quantitative PCR was performed in technical triplicates using the MESA GREEN qPCR MasterMix Plus for SYBR (Eurogentec). The geometric mean of ChIP signals at two irrelevant loci (P4, M40) was used as a negative control. At least two independent biological experiments were performed.

The primers used are listed in Table S3.

RNA-seq

Samples were prepared from 3 biological replicates of *Δcbf11* (MP44) and *cbf11DBM-TAP* (MP712) cells and 4 biological replicates of WT (JB32). Cells were cultured to exponential phase, 10 mL were harvested (600 g, 2 min) and the cell pellet was flash-frozen. Total RNA was isolated using a hot acidic phenol method followed by phenol-chloroform extractions and precipitation (Lyne et al., 2003). Extracted RNA was treated with TURBO DNase (Thermo Fisher Scientific) and purified using Qiagen RNeasy columns. RNA quality was assessed on Agilent Bioanalyzer.

3 samples of each *Δcbf11* and WT were processed at the CCGA (Competence Centre for Genomic Analysis), Christian-Albrechts-University Kiel, Germany. Libraries were prepared using the Illumina TruSeq stranded mRNA Library (poly-A), and sequenced in the pair-end mode on an Illumina NovaSeq 6000 instrument with the NovaSeq 6000 SP Reagent Kit with 100 cycles. The remaining 3 samples of *cbf11DBM-TAP* and 1 sample of WT were processed separately at the Institute of Molecular Genetics (IMG, Czech Academy of Sciences, Prague). The sequencing libraries were synthesized using KAPA mRNA HyperPrep Kit (Illumina platform) (Roche, KK8581) and analyzed on an Illumina NextSeq 500 instrument using the NextSeq 500/550 High Output Kit v2.5 (75 Cycles) (Illumina) with single-end, 75 bp, dual index setup.

RNA-seq data analysis

The reference *S. pombe* genome and annotation were downloaded from PomBase (2022-05-30; https://www.pombase.org/; (Lock et al., 2019; Wood et al., 2002)). Read quality was checked using FastQC version 0.11.9 (https://www.bioinformatics.babraham.ac.uk/projects/fastqc/). Adapters and low-quality sequences were removed using Trimmomatic 0.39 (Bolger et al., 2014). Clean reads were aligned to the *S. pombe* genome using HISAT2 2.2.1 (Kim et al., 2015) and SAMtools 1.13 (Bonfield et al., 2021; Li et al., 2009). Read coverage tracks were then computed and normalized to the respective mapped library sizes using deepTools 3.5.1 (Ramírez et al., 2016). Mapped reads and coverage data were inspected visually in the IGV 2.9 browser (Robinson et al., 2011). Differentially expressed genes were detected using the RUVseq and DESeq2 packages (Love et al., 2014; Risso et al., 2014) in R/Bioconductor (Gentleman et al., 2004; Huber et al., 2015).

ChIP-nexus

For Cbf11-related analyses, 400 mL cultures of Cbf11-TAP (MP707), Cbf11DBM-TAP (MP712), untagged WT (JB32, a negative control) and Fkh2-TAP (MP931, forkhead transcription factor unrelated to CSL; a negative control) cells were grown in YES to exponential phase. For Cbf12-related analyses, 10-15 mL of Cbf12-TAP (MP540), Cbf12DBM-TAP (MP518), untagged WT (JB32) and Fkh2-TAP (MP931) cells were grown in YES to stationary phase and were brought up to 400 mL with YES before fixation. Three independent biological experiments were performed for the CSL proteins; the negative controls were grown once for each cultivation condition.

Saccharomyces cerevisiae cells expressing the histone H2A.2-TAP (Euroscarf yeast strain collection, original ID SC0421, lab ID MP792) were used as a potential spike-in control for normalization of ChIP samples of TAP-tagged *S. pombe* proteins. *S. cerevisiae* cells were cultivated to exponential phase (OD_{600} 1.8) in the complex YPAD medium at 30°C, and chromatin extract preparation was performed as described below for *S. pombe* with these exceptions: fixation for 30 min, 15 cycles of chromatin shearing. However, after assessing the performance of the spike-in control, we decided not to take it into account during subsequent data analyses.

Cells were fixed by adding formaldehyde to the final concentration of 1%. After 10 min incubation, the remaining formaldehyde was quenched by 125 mM glycine for 10 min. Cells were washed with PBS and broken with glass beads in the Lysis Buffer (50 mM Hepes pH 7.6, 1 mM EDTA pH 8.0, 150 mM NaCl, 1% Triton X-100, 0.1% sodium deoxycholate, FY protease inhibitors [Serva], 1 mM PMSF) using the FastPrep24 machine (MP Biomedicals). Extracted chromatin was sheared with the Bioruptor sonicator (Diagenode) using 20 cycles of 30 s on, 30 s off at high power settings. An aliquot of each chromatin extract was kept as the input control sample (used for a qPCR validation step), and 1.5-2 mg of chromatin extract with added *S. cerevisiae* spike-in chromatin (40,000-fold dilution) were used for immunoprecipitation with 100 µl of BSA-blocked magnetic IgG-coated beads (Invitrogen, 110.41). Chromatin immunoprecipitation was performed on a rotating wheel overnight at 4°C. The precipitated material was ChIP-exo treated according to the updated, simplified version of the ChIP-nexus approach (ChIP-nexus [version 2019]; https://research.stowers.org/zeitlingerlab/protocols.html) introduced by (He et al., 2015), except for wash buffers A-D that were optimized for yeasts as previously described (Doris et al., 2018). ChIP-exo treated material was eluted in Elution Buffer (50 mM Tris-HCl pH 8.0, 10 mM EDTA, 1% SDS). Cross-links were reversed at 65°C for 6 h, samples were treated with DNase-free RNase A followed by proteinase K digestion, and purified using standard phenol-chloroform extraction and sodium acetate/ethanol precipitation. qPCR was performed to check the efficiency of ChIP. ChIP-nexus library construction for Illumina sequencing was performed as described in the updated version of the ChIP-nexus approach (see above). Concentration of ChIP-nexus libraries was measured using the Quantus fluorometer (Promega) and fragment size distribution was checked on Agilent Bioanalyzer using the High Sensitivity DNA Assay. Libraries were pooled and sequenced in two technical-repeat runs on an Illumina NextSeq 500 instrument (75 nt single-end mode) using the NextSeq 500/550 High Output Reagent Cartridge v2 (75 cycles) by the Genomics and Bioinformatics service facility at the Institute of Molecular Genetics (Czech Academy of Sciences, Prague). The list of used ChIP-nexus oligonucleotides is provided in Table S4.

ChIP-nexus data analysis

The reference *S. pombe* and *S. cerevisiae* genome and annotation were downloaded from PomBase (2022-05-30; https://www.pombase.org/; (Lock et al., 2019; Wood et al., 2002)). Read quality was checked using FastQC version 0.11.9 (https://www.bioinformatics.babraham.ac.uk/projects/fastqc/). Adapters and low-quality sequences were removed using Trimmomatic 0.39 (Bolger et al., 2014). Reads without an intact, correctly positioned nexus barcode were discarded. Clean reads were

aligned to a hybrid *S. pombe & S. cerevisiae* genome using HISAT2 2.2.1 (Kim et al., 2015) and SAMtools 1.13 (Bonfield et al., 2021; Li et al., 2009). PCR duplicates were removed based on unique molecule identifiers (UMI) and mapping information. Read coverage tracks were then computed and normalized to the respective mapped library sizes using deepTools 3.5.1 (Ramírez et al., 2016). Mapped reads and coverage data were inspected visually in the IGV 2.9 browser (Robinson et al., 2011). Peak calling was performed using MACS3 (version 3.0.0a7) (Zhang et al., 2008). Only reproducible peaks present in all three replicates, but absent from the negative control ChIPs (untagged WT, Fkh2-TAP) were kept.

Expression microarrays

WT (JB32), *Δcbf11* (MP44), and *Δcbf12* (MP21) cells were grown to exponential phase (OD ~0.5) in YES. Fifty milliliters of untreated cultures were harvested as controls. Another 50 mL of each culture was treated with 20 μM CPT (with DMSO added to 1%) for 2 hours and harvested. The experiment was performed twice. Total RNA was extracted and analyzed using custom-designed Agilent 44K two-color expression microarrays as described previously (Převorovský et al., 2015). Samples were hybridized against a control sample created by pooling aliquots from all 12 samples.

Western blot analysis

To test Chk1 activation by CPT, 20 mL cultures of Chk1-13Myc (WT; MP287), Chk1-13Myc *Δcbf11* (*Δcbf11*; MP304), Chk1-13Myc *Δcbf12* (*Δcbf12*; MP291), and untagged WT (JB32, a negative control) cells were grown in YES to exponential phase. 10 mL of cells were harvested by centrifugation, washed with STOP buffer (150 mM NaCl, 50 mM NaF, 25 mM HEPES, 1 mM NaN_3; pH 8) and kept at -80°C. The remaining 10 mL of cultures were treated with 20 μM CPT (DMSO to 1%) for 2 hours and then harvested. Native protein extracts were prepared in NP-40 buffer (6 mM Na_2HPO_4, 4 mM $NaH_2PO_4 \cdot H_2O$, 1% NONIDET P-40, 150 mM NaCl, 2 mM EDTA, 50 mM NaF, FY protease inhibitors [Serva], phosphatase inhibitors (Sigma cocktails 2+3; P5726, P0044); pH 7.6) by breaking the cells with glass beads in a FastPrep24 instrument (MP Biomedicals).

Proteins were separated on a 7.5% Tris-glycine polyacrylamide gel, transferred to a nitrocellulose membrane and probed with a mouse monoclonal anti-Myc antibody (MMS-150P, Covance, 1:1000). A goat-anti-mouse alkaline phosphatase-conjugated secondary antibody (170–6520, Bio-Rad, 1:3000) was used for detection (Fig. 4F, S6). Two independent biological replicates were performed.

Pulsed Field Gel Electrophoresis (PFGE)

Intact chromosomes from WT (JB32) cells and two freshly prepared clones of *Δcbf11* (MP274, MP275) were analyzed by PFGE technique as described previously (Yamada et al., 2020; Zaratiegui et al., 2011). Four independent colonies per strain were analyzed (Fig. S5). PFGE analysis of rDNA arrays followed by southern blot probed for rDNA was performed with PvuII-digested DNA from WT (JB32), *Δcbf11* (MP267), and *Δcbf12* (MP266) cells (Fig. 7C). Note that no PvuII restriction sites are

present in the rDNA sequence (Barnitz et al., 1982). At least 2 independent biological replicates were performed.

DATA AVAILABILITY

Source data for Figures, including the numbers of independent experiments (n) in bar plots (Fig. 1C, 2B, 3B, 3C, 7D, 7F, Fig. S1) are available as Supplementary File 2.
The sequencing and microarray data are available from the ArrayExpress database (https://www.ebi.ac.uk/arrayexpress/) under the accession numbers E-MTAB-13305 and E-MTAB-13302 (RNA-seq), E-MTAB-13258 (ChIP-nexus), and E-MTAB-13621 (microarrays), respectively. Previously published ChIP-seq data (H3K9 acetylation in lipid metabolism mutants) (Princová et al., 2023; Vishwanatha et al., 2023) were obtained from ArrayExpress (accession numbers E-MTAB-11081, E-MTAB-11082). Previously published ChIP-seq data for TAP-tagged CSL proteins (Převorovský et al., 2015) were obtained from ArrayExpress (accession number E-MTAB-2725).
The scripts used for sequencing data processing and analyses are available from https://github.com/mprevorovsky/CSL-DBM-paper.

FUNDING

This work was supported by the Grant Agency of Charles University (GA UK grant no. 248120 to A.M.). M.H. was supported by the European Union - Next Generation EU (programme EXCELES project no. LX22NPO5102). Parts of the sequencing analysis were supported by the DFG Research Infrastructure NGS CC (project 407495230) as part of the Next Generation Sequencing Competence Network (project 423957469). These parts of the NGS analysis were carried out at the Competence Centre for Genomic Analysis (Kiel, Germany).

ACKNOWLEDGEMENTS

We would like to thank the Yeast Genetic Resource Center Japan (NBRP Japan) for providing the *fkh2-TAP* strain (FY32982), the Euroscarf collection center (distributed by Scientific Research and Development GmbH; Germany) for providing the *S. cerevisiae H2A.2-TAP* strain (SC0421), and Kazunori Tomita for the *chk1-13Myc* and *hht1-mRFP* strains. We are grateful to Štěpánka Hrdá and Blanka Hamplová from the Genomics core facility at Biocev Research Center, Faculty of Science, Charles University for Sanger sequencing and quality control of nucleic acids; Valeria Buccheri for help with optimizing the ChIP-nexus protocol; Ondřej Šebesta for creating the ImageJ script for nuclei extraction from the microscopy images; Adéla Kracíková, Kateřina Svobodová and Eva Krellerová for excellent technical assistance; all members of the GenoMik and ReGenEx groups for their support and insightful discussions. Microscopy was performed in the Vinicna Microscopy Core Facility co-financed by the Czech-BioImaging large RI project LM2023050. Computational resources were supplied by the project "e-Infrastruktura CZ" (e-INFRA LM2018140) provided within the program Projects of Large Research, Development and Innovations Infrastructures.

COMPETING INTERESTS

No competing interests declared.

REFERENCE LIST

Anderson, H. E., Wardle, J., Korkut, S. V., Murton, H. E., López-Maury, L., Bähler, J. and Whitehall, S. K. (2009). The fission yeast HIRA histone chaperone is required for promoter silencing and the suppression of cryptic antisense transcripts. *Mol. Cell. Biol.* **29**, 5158–67.

Atkinson, S. R., Marguerat, S., Bitton, D. A., Rodríguez-López, M., Rallis, C., Lemay, J.-F., Cotobal, C., Malecki, M., Smialowski, P., Mata, J., et al. (2018). Long noncoding RNA repertoire and targeting by nuclear exosome, cytoplasmic exonuclease, and RNAi in fission yeast. *RNA* **24**, 1195–1213.

Bähler, J., Wu, J. Q., Longtine, M. S., Shah, N. G., McKenzie, A., Steever, A. B., Wach, A., Philippsen, P. and Pringle, J. R. (1998). Heterologous modules for efficient and versatile PCR-based gene targeting in Schizosaccharomyces pombe. *Yeast* **14**, 943–51.

Barnitz, J. T., Cramer, J. H., Rownd, R. H., Cooley, L. and Söll, D. (1982). Arrangement of the ribosomal RNA genes in Schizosaccharomyces pombe. *FEBS Lett.* **143**, 129–32.

Bolger, A. M., Lohse, M. and Usadel, B. (2014). Trimmomatic: a flexible trimmer for Illumina sequence data. *Bioinformatics* **30**, 2114–20.

Bonfield, J. K., Marshall, J., Danecek, P., Li, H., Ohan, V., Whitwham, A., Keane, T. and Davies, R. M. (2021). HTSlib: C library for reading/writing high-throughput sequencing data. *Gigascience* **10**, 1–6.

Borggrefe, T. and Oswald, F. (2009). The Notch signaling pathway: transcriptional regulation at Notch target genes. *Cell. Mol. Life Sci.* **66**, 1631–46.

Bottoni, G., Katarkar, A., Tassone, B., Ghosh, S., Clocchiatti, A., Goruppi, S., Bordignon, P., Jafari, P., Tordini, F., Lunardi, T., et al. (2019). CSL controls telomere maintenance and genome stability in human dermal fibroblasts. *Nat. Commun.* **10**, 3884.

Burr, R., Stewart, E. V., Shao, W., Zhao, S., Hannibal-Bach, H. K., Ejsing, C. S. and Espenshade, P. J. (2016). Mga2 Transcription Factor Regulates an Oxygen-responsive Lipid Homeostasis Pathway in Fission Yeast. *J. Biol. Chem.* **291**, 12171–83.

Burr, R., Stewart, E. V. and Espenshade, P. J. (2017). Coordinate Regulation of Yeast Sterol Regulatory Element-binding Protein (SREBP) and Mga2 Transcription Factors. *J. Biol. Chem.* **292**, 5311–5324.

Chen, D., Toone, W. M., Mata, J., Lyne, R., Burns, G., Kivinen, K., Brazma, A., Jones, N. and Bähler, J. (2003). Global transcriptional responses of fission yeast to environmental stress. *Mol. Biol. Cell* **14**, 214–29.

Chung, C. N., Hamaguchi, Y., Honjo, T. and Kawaichi, M. (1994). Site-directed mutagenesis study on DNA binding regions of the mouse homologue of Suppressor of Hairless, RBP-J kappa. *Nucleic Acids Res.* **22**, 2938–44.

de Bruin, R. a M., Kalashnikova, T. I., Aslanian, A., Wohlschlegel, J., Chahwan, C., Yates, J. R., Russell, P. and Wittenberg, C. (2008). DNA replication checkpoint promotes G1-S transcription by inactivating the MBF repressor Nrm1. *Proc. Natl. Acad. Sci. U. S. A.* **105**, 11230–5.

Deshpande, G. P., Hayles, J., Hoe, K.-L., Kim, D.-U., Park, H.-O. and Hartsuiker, E. (2009). Screening a genome-wide S. pombe deletion library identifies novel genes and pathways involved in genome stability maintenance. *DNA Repair (Amst).* **8**, 672–9.

Doris, S. M., Chuang, J., Viktorovskaya, O., Murawska, M., Spatt, D., Churchman, L. S. and Winston, F. (2018). Spt6 Is Required for the Fidelity of Promoter Selection. *Mol. Cell* **72**, 687-699.e6.

Gagliani, E. K., Gutzwiller, L. M., Kuang, Y., Odaka, Y., Hoffmeister, P., Hauff, S., Turkiewicz, A., Harding-Theobald, E., Dolph, P. J., Borggrefe, T., et al. (2022). A Drosophila Su(H) model of Adams-Oliver Syndrome reveals cofactor titration as a mechanism underlying developmental defects. *PLoS Genet.* **18**, e1010335.

Gentleman, R. C., Carey, V. J., Bates, D. M., Bolstad, B., Dettling, M., Dudoit, S., Ellis, B., Gautier, L., Ge, Y., Gentry, J., et al. (2004). Bioconductor: open software development for computational biology and bioinformatics. *Genome Biol.* **5**, R80.

Hall, D. P. and Kovall, R. A. (2019). Structurally conserved binding motifs of transcriptional regulators to notch nuclear effector CSL. *Exp. Biol. Med. (Maywood).* **244**, 1520–1529.

Han, T. X., Xu, X.-Y., Zhang, M.-J., Peng, X. and Du, L.-L. (2010). Global fitness profiling of fission yeast deletion strains by barcode sequencing. *Genome Biol.* **11**, R60.

He, Q., Johnston, J. and Zeitlinger, J. (2015). ChIP-nexus enables improved detection of in vivo transcription factor binding footprints. *Nat. Biotechnol.* **33**, 395–401.

Hori, Y., Engel, C. and Kobayashi, T. (2023). Regulation of ribosomal RNA gene copy number, transcription and nucleolus organization in eukaryotes. *Nat. Rev. Mol. Cell Biol.* **24**, 414–429.

Huber, W., Carey, V. J., Gentleman, R., Anders, S., Carlson, M., Carvalho, B. S., Bravo, H. C., Davis, S., Gatto, L., Girke, T., et al. (2015). Orchestrating high-throughput genomic analysis with Bioconductor. *Nat. Methods* **12**, 115–21.

Ide, S., Miyazaki, T., Maki, H. and Kobayashi, T. (2010). Abundance of ribosomal RNA gene copies maintains genome integrity. *Science* **327**, 693–6.

Kato, H., Taniguchi, Y., Kurooka, H., Minoguchi, S., Sakai, T., Nomura-Okazaki, S., Tamura, K. and Honjo, T. (1997). Involvement of RBP-J in biological functions of mouse Notch1 and its derivatives. *Development* **124**, 4133–41.

Kim, D., Langmead, B. and Salzberg, S. L. (2015). HISAT: a fast spliced aligner with low memory requirements. *Nat. Methods* **12**, 357–60.

Kobayashi, T. (2011). Regulation of ribosomal RNA gene copy number and its role in modulating genome integrity and evolutionary adaptability in yeast. *Cell. Mol. Life Sci.* **68**, 1395–403.

Kobayashi, T., Heck, D. J., Nomura, M. and Horiuchi, T. (1998). Expansion and contraction of ribosomal DNA repeats in Saccharomyces cerevisiae: requirement of replication fork blocking (Fob1) protein and the role of RNA polymerase I. *Genes Dev.* **12**, 3821–30.

Kovall, R. a and Hendrickson, W. a (2004). Crystal structure of the nuclear effector of Notch signaling, CSL, bound to DNA. *EMBO J.* **23**, 3441–51.

Kwon, E. G., Laderoute, A., Chatfield-Reed, K., Vachon, L., Karagiannis, J. and Chua, G. (2012). Deciphering the transcriptional-regulatory network of flocculation in Schizosaccharomyces pombe. *PLoS Genet.* **8**, e1003104.

Lee, Y.-H., Nadaraia, S., Gu, D., Becker, D. F. and Tanner, J. J. (2003). Structure of the proline dehydrogenase domain of the multifunctional PutA flavoprotein. *Nat. Struct. Biol.* **10**, 109–14.

Li, H., Handsaker, B., Wysoker, A., Fennell, T., Ruan, J., Homer, N., Marth, G., Abecasis, G., Durbin, R. and 1000 Genome Project Data Processing Subgroup (2009). The Sequence Alignment/Map format and SAMtools. *Bioinformatics* **25**, 2078–9.

Linder, T. and Gustafsson, C. M. (2008). Molecular phylogenetics of ascomycotal adhesins--a novel family of putative cell-surface adhesive proteins in fission yeasts. *Fungal Genet. Biol.* **45**, 485–97.

Lock, A., Rutherford, K., Harris, M. A., Hayles, J., Oliver, S. G., Bähler, J. and Wood, V. (2019). PomBase 2018: user-driven reimplementation of the fission yeast database provides rapid and intuitive access to diverse, interconnected information. *Nucleic Acids Res.* **47**, D821–D827.

Love, M. I., Huber, W. and Anders, S. (2014). Moderated estimation of fold change and dispersion for RNA-seq data with DESeq2. *Genome Biol.* **15**, 550.

Lyne, R., Burns, G., Mata, J., Penkett, C. J., Rustici, G., Chen, D., Langford, C., Vetrie, D. and Bähler, J. (2003). Whole-genome microarrays of fission yeast: characteristics, accuracy, reproducibility, and processing of array data. *BMC Genomics* **4**, 27.

Makarova, M., Gu, Y., Chen, J.-S., Beckley, J. R., Gould, K. L. and Oliferenko, S. (2016). Temporal Regulation of Lipin Activity Diverged to Account for Differences in Mitotic Programs. *Curr. Biol.* **26**, 237–243.

Marguerat, S., Schmidt, A., Codlin, S., Chen, W., Aebersold, R. and Bähler, J. (2012). Quantitative analysis of fission yeast transcriptomes and proteomes in proliferating and quiescent cells. *Cell* **151**, 671–83.

Mejía-Ramírez, E., Sánchez-Gorostiaga, A., Krimer, D. B., Schvartzman, J. B. and Hernández, P. (2005). The mating type switch-activating protein Sap1 Is required for replication fork arrest at the rRNA genes of fission yeast. *Mol. Cell. Biol.* **25**, 8755–61.

Nicolas, E., Yamada, T., Cam, H. P., Fitzgerald, P. C., Kobayashi, R. and Grewal, S. I. S. (2007). Distinct roles of HDAC complexes in promoter silencing, antisense suppression and DNA damage protection. *Nat. Struct. Mol. Biol.* **14**, 372–80.

Noguchi, E., Ansbach, A. B., Noguchi, C. and Russell, P. (2009). Assays used to study the DNA replication checkpoint in fission yeast. *Methods Mol. Biol.* **521**, 493–507.

Okazaki, K., Okazaki, N., Kume, K., Jinno, S., Tanaka, K. and Okayama, H. (1990). High-frequency transformation method and library transducing vectors for cloning mammalian cDNAs by trans-complementation of Schizosaccharomyces pombe. *Nucleic Acids Res.* **18**, 6485–9.

Oravcová, M., Teska, M., Půta, F., Folk, P. and Převorovský, M. (2013). Fission yeast CSL proteins function as transcription factors. *PLoS One* **8**, e59435.

Pan, X., Lei, B., Zhou, N., Feng, B., Yao, W., Zhao, X., Yu, Y. and Lu, H. (2012). Identification of novel genes involved in DNA damage response by screening a genome-wide Schizosaccharomyces pombe deletion library. *BMC Genomics* **13**, 662.

Petersen, J. and Russell, P. (2016). Growth and the Environment of Schizosaccharomyces pombe. *Cold Spring Harb. Protoc.* **2016**, pdb.top079764.

Převorovský, M., Půta, F. and Folk, P. (2007). Fungal CSL transcription factors. *BMC Genomics* **8**, 233.

Převorovský, M., Groušl, T., Staňurová, J., Ryneš, J., Nellen, W., Půta, F. and Folk, P. (2009). Cbf11 and Cbf12, the fission yeast CSL proteins, play opposing roles in cell adhesion and coordination of cell and nuclear division. *Exp. Cell Res.* **315**, 1533–47.

Převorovský, M., Oravcová, M., Tvarůžková, J., Zach, R., Folk, P., Půta, F. and Bähler, J. (2015). Fission Yeast CSL Transcription Factors: Mapping Their Target Genes and Biological Roles. *PLoS One* **10**, e0137820.

Převorovský, M., Oravcová, M., Zach, R., Jordáková, A., Bähler, J., Půta, F. and Folk, P. (2016). CSL protein regulates transcription of genes required to prevent catastrophic mitosis in fission yeast. *Cell Cycle* **15**, 3082–3093.

Princová, J., Schätz, M., Ťupa, O. and Převorovský, M. (2019). Analysis of Lipid Droplet Content in Fission and Budding Yeasts using Automated Image Processing. *J. Vis. Exp.* 1–9.

Princová, J., Salat-Canela, C., Daněk, P., Marešová, A., de Cubas, L., Bähler, J., Ayté, J., Hidalgo, E. and Převorovský, M. (2023). Perturbed fatty-acid metabolism is linked to localized chromatin hyperacetylation, increased stress-response gene expression and resistance to oxidative stress. *PLoS Genet.* **19**, e1010582.

Ramírez, F., Ryan, D. P., Grüning, B., Bhardwaj, V., Kilpert, F., Richter, A. S., Heyne, S., Dündar, F. and Manke, T. (2016). deepTools2: a next generation web server for deep-sequencing data analysis. *Nucleic Acids Res.* **44**, W160-5.

Risso, D., Ngai, J., Speed, T. P. and Dudoit, S. (2014). Normalization of RNA-seq data using factor analysis of control genes or samples. *Nat. Biotechnol.* **32**, 896–902.

Robinson, J. T., Thorvaldsdóttir, H., Winckler, W., Guttman, M., Lander, E. S., Getz, G. and Mesirov, J. P. (2011). Integrative genomics viewer. *Nat. Biotechnol.* **29**, 24–6.

Rodriguez-Lopez, M., Anver, S., Cotobal, C., Kamrad, S., Malecki, M., Correia-Melo, C., Hoti, M., Townsend, S., Marguerat, S., Pong, S. K., et al. (2022). Functional profiling of long intergenic non-coding RNAs in fission yeast. *Elife* **11**, 1–27.

Rozenzhak, S., Mejía-Ramírez, E., Williams, J. S., Schaffer, L., Hammond, J. A., Head, S. R. and Russell, P. (2010). Rad3 decorates critical chromosomal domains with gammaH2A to protect genome integrity during S-Phase in fission yeast. *PLoS Genet.* **6**, e1001032.

Rustici, G., Mata, J., Kivinen, K., Lió, P., Penkett, C. J., Burns, G., Hayles, J., Brazma, A., Nurse, P. and Bähler, J. (2004). Periodic gene expression program of the fission yeast cell cycle. *Nat. Genet.* **36**, 809–17.

Sabatinos, S. A. and Forsburg, S. L. (2010). Molecular genetics of Schizosaccharomyces pombe. *Methods Enzymol.* **470**, 759–95.

Sánchez-Gorostiaga, A., López-Estraño, C., Krimer, D. B., Schvartzman, J. B. and Hernández, P. (2004). Transcription termination factor reb1p causes two replication fork barriers at its cognate sites in fission yeast ribosomal DNA in vivo. *Mol. Cell. Biol.* **24**, 398–406.

Schneider, C. A., Rasband, W. S. and Eliceiri, K. W. (2012). NIH Image to ImageJ: 25 years of Image Analysis HHS Public Access. *Nat Methods* **9**, 671–675.

Singh, A. and Xu, Y.-J. (2016). The Cell Killing Mechanisms of Hydroxyurea. *Genes (Basel).* **7**,.

Singh, S. K., Sabatinos, S., Forsburg, S. and Bastia, D. (2010). Regulation of replication termination by Reb1 protein-mediated action at a distance. *Cell* **142**, 868–78.

Takemoto, A., Kawashima, S. A., Li, J.-J., Jeffery, L., Yamatsugu, K., Elemento, O. and Nurse, P. (2016). Nuclear envelope expansion is crucial for proper chromosomal segregation during a closed mitosis. *J. Cell Sci.* **129**, 1250–9.

Vachon, L., Wood, J., Kwon, E.-J. G., Laderoute, A., Chatfield-Reed, K., Karagiannis, J. and Chua, G. (2013). Functional characterization of fission yeast transcription factors by overexpression analysis. *Genetics* **194**, 873–84.

Vishwanatha, A., Princová, J., Hohoš, P., Zach, R. and Převorovský, M. (2023). Altered cohesin dynamics and H3K9 modifications contribute to mitotic defects in the cbf11Δ lipid metabolism mutant. *J. Cell Sci.*

Volpe, T. A., Kidner, C., Hall, I. M., Teng, G., Grewal, S. I. S. and Martienssen, R. A. (2002). Regulation of heterochromatic silencing and histone H3 lysine-9 methylation by RNAi. *Science* **297**, 1833–7.

Wan, S., Capasso, H. and Walworth, N. C. (1999). The topoisomerase I poison camptothecin generates a Chk1-dependent DNA damage checkpoint signal in fission yeast. *Yeast* **15**, 821–8.

Watson, A., Mata, J., Bähler, J., Carr, A. and Humphrey, T. (2004). Global gene expression responses of fission yeast to ionizing radiation. *Mol. Biol. Cell* **15**, 851–60.

Wegrzyn, J., Potla, R., Chwae, Y.-J., Sepuri, N. B. V, Zhang, Q., Koeck, T., Derecka, M., Szczepanek, K., Szelag, M., Gornicka, A., et al. (2009). Function of mitochondrial Stat3 in cellular respiration. *Science* **323**, 793–7.

Wells, M. L., Huang, W., Li, L., Gerrish, K. E., Fargo, D. C., Ozsolak, F. and Blackshear, P. J. (2012). Posttranscriptional regulation of cell-cell interaction protein-encoding transcripts by Zfs1p in Schizosaccharomyces pombe. *Mol. Cell. Biol.* **32**, 4206–14.

Wood, V., Gwilliam, R., Rajandream, M.-A., Lyne, M., Lyne, R., Stewart, A., Sgouros, J., Peat, N., Hayles, J., Baker, S., et al. (2002). The genome sequence of Schizosaccharomyces pombe. *Nature* **415**, 871–80.

Yamada, T., Murakami, H. and Ohta, K. (2020). Pulsed-Field Gel Electrophoresis for Detecting Chromosomal DNA Breakage in Fission Yeast. In *Current Opinion in Biotechnology*, pp. 135–143.

Yanagida, M. (1998). Fission yeast cut mutations revisited: control of anaphase. *Trends Cell Biol.* **8**, 144–9.

Zach, R. and Převorovský, M. (2018). The phenomenon of lipid metabolism “cut” mutants. *Yeast* **35**, 631–637.

Zach, R., Tvarůžková, J., Schätz, M., Ťupa, O., Grallert, B. and Převorovský, M. (2018). Mitotic defects in fission yeast lipid metabolism “cut” mutants are suppressed by ammonium chloride. *FEMS Yeast Res.* **18**, 1–7.

Zaratiegui, M., Vaughn, M. W., Irvine, D. V, Goto, D., Watt, S., Bähler, J., Arcangioli, B. and Martienssen, R. A. (2011). CENP-B preserves genome integrity at replication forks paused by retrotransposon LTR. *Nature* **469**, 112–115.

Zhang, Y., Liu, T., Meyer, C. A., Eeckhoute, J., Johnson, D. S., Bernstein, B. E., Nusbaum, C., Myers, R. M., Brown, M., Li, W., et al. (2008). Model-based analysis of ChIP-Seq (MACS). *Genome Biol.* **9**, R137.

Figures

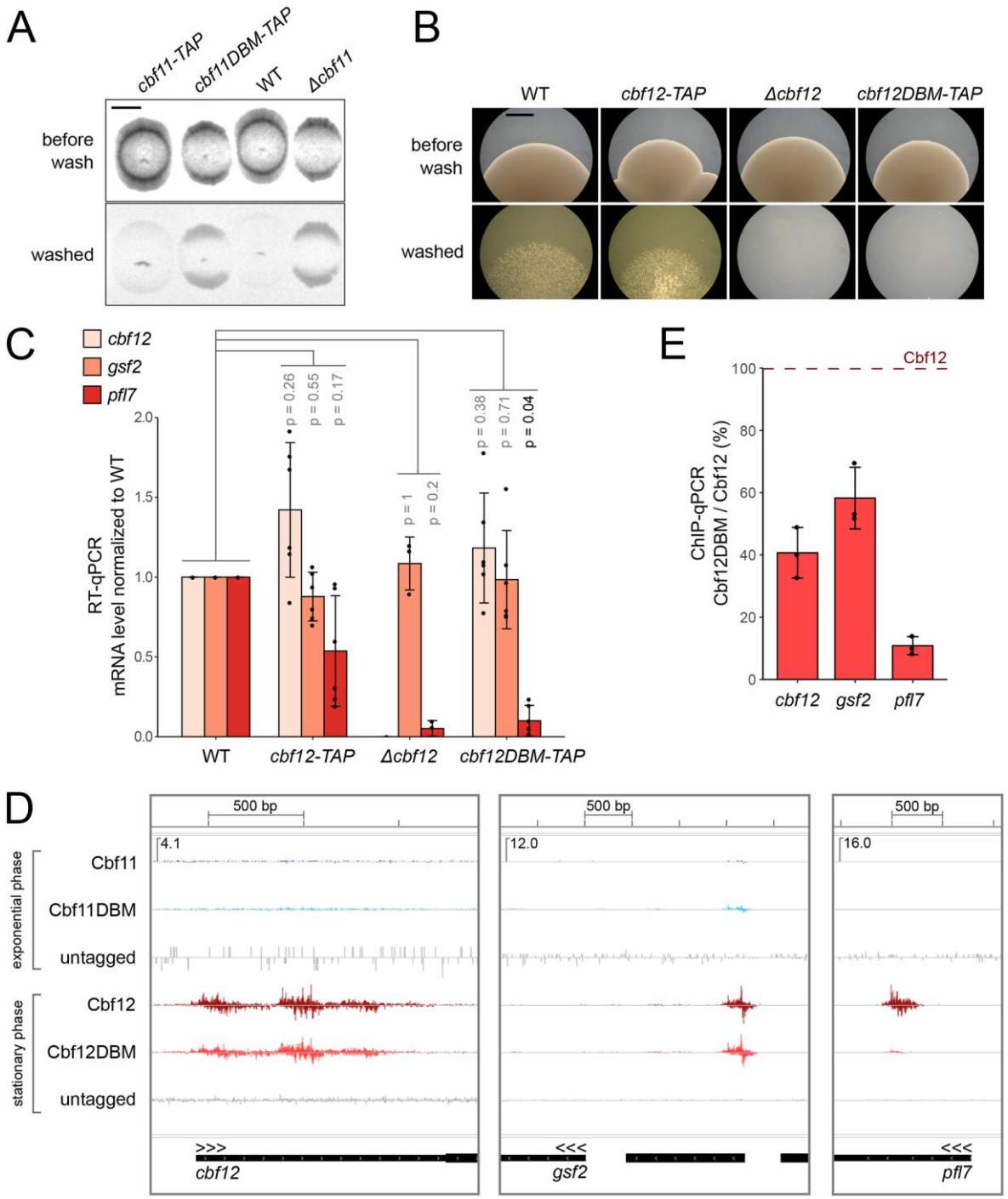

Fig. 1. DNA-binding activities of CSL proteins are required for their antagonism in cell adhesion.

A) Both *Δcbf11* and *cbf11DBM-TAP* cells display higher adhesion to agar than WT and *cbf11-TAP* cells. Cells were spotted on a plate, incubated at 32°C for 8 days, and then washed with a stream of water. Whole spots were imaged before and after

washing. Images representative of 2 independent experiments are shown. Brightness and contrast were adjusted for clarity. Scale bar represents 5 mm.

B) Cells lacking *cbf12* as well as *cbf12DBM-TAP* cells do not adhere to agar. Cells growing for 7 days on a plate were subjected to a washing test. A microscopic picture of the colony edge was taken before and after washing. Images representative of 3 independent experiments are shown. Scale bar represents 0.5 mm.

C) Expression of the indicated adhesion-related genes in WT, *cbf12-TAP*, *Δcbf12*, and *cbf12DBM-TAP* cells grown to stationary phase was analyzed by RT-qPCR. Mean ± SD values, as well as individual data points for ≥2 independent experiments are shown. Two-sided Mann-Whitney U test was used to determine statistical significance. Note that the change of *pfl7* mRNA level in *Δcbf12* is not statistically significant because only two measurements were done.

D) *In vivo* binding of TAP-tagged CSL proteins to the promoters of indicated adhesion genes was analyzed by ChIP-nexus. Mean strand-specific coverage profile of 3 independent experiments for Cbf11/12 and Cbf11DBM/12DBM, and a strand-specific coverage profile for untagged WT cells (negative control) were visualized in the Integrated Genome Viewer (IGV; Broad Institute). Gene orientation is indicated by three arrowheads; all sample tracks have the same Y-axis scaling, with the maximum Y-axis value for each locus given in the top-left corner.

E) ChIP-qPCR shows the decrease in DNA binding of the Cbf12DBM-TAP protein compared to its unmutated counterpart at selected target loci in the stationary phase. Mean ± SD values, and individual data points of 3 independent replicates are shown.

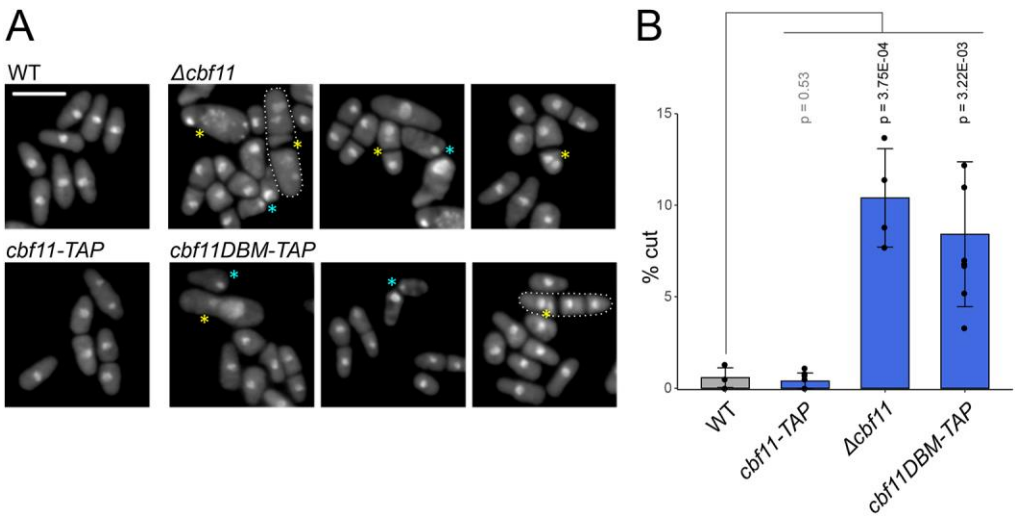

Fig. 2. Cbf11DBM cells display the same mitotic and morphology defects as *Δcbf11* cells.

A) Microscopy of ethanol-fixed, DAPI-stained (nuclei) cells from exponential phase. Images representative of 4 independent experiments. *cbf11DBM-TAP* cells resemble *Δcbf11*: aberrant morphology of cells and nuclei, fragmentation of the nuclear mass (yellow asterisks), “cut” phenotype (cyan asterisks). Scale bar represents 10 µm.

B) Quantification of the occurrence of the “cut” phenotype in cells from panel A. Both *Δcbf11* and *cbf11DBM-TAP* mutants display the “cut” phenotype with similar penetrance. Mean ± SD values, as well as individual data points for ≥4 independent experiments are shown. Significance was determined by a two-tailed unpaired t-test.

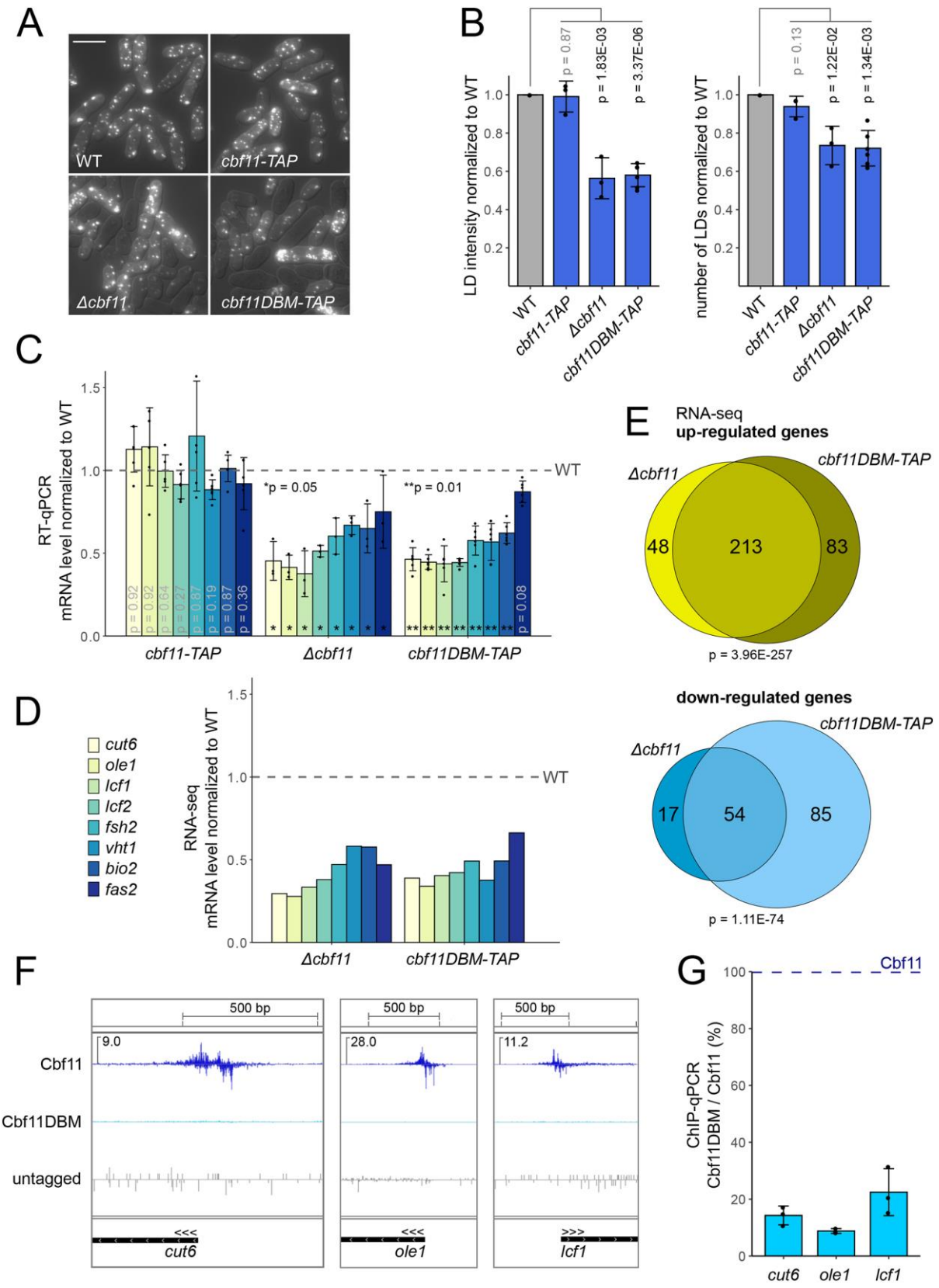

Fig. 3. Intact DNA-binding domain of Cbf11 is necessary for its role in lipid metabolism regulation.

A) Lipid droplet (LD) formation in exponentially growing cells. Both *Δcbf11* and *cbf11DBM-TAP* mutants display decreased LD content and heterogeneity. Microscopic images representative of 3 independent experiments of live cells with LDs stained with BODIPY 493/503. DIC overlay is shown to mark cell boundaries. Scale bar represents 10 μm.

B) Total fluorescence intensity (left) and number of identified LDs (right) per unit of cell volume. Mean ± SD values, as well as individual data points for ≥3 independent experiments are shown. Significance was determined by a two-tailed unpaired t-test.

C) Expression of selected lipid-related genes in the indicated cells grown to the exponential phase was analyzed by RT-qPCR. mRNA levels are significantly decreased (except for *fas2*) in *Δcbf11* and *cbf11DBM-TAP* cells compared to WT. Mean ± SD values, as well as individual data points for ≥3 independent experiments are shown. One-sided Mann-Whitney U test was used to determine statistical significance. The legend is shared with panel D.

D) Expression of the lipid-related genes from panel C determined by RNA-seq. Mean values for 3 independent experiments are shown.

E) Venn diagram of genes showing differential expression in *Δcbf11* and *cbf11DBM-TAP* cells. Only protein-coding genes showing at least 2-fold and statistically significant change in expression compared to WT are included. Overlap significance was determined using Fisher's exact test.

F) *In vivo* binding of Cbf11 and Cbf11DBM TAP-tagged proteins to the promoters of selected lipid-related genes in the exponential phase was analyzed by ChIP-nexus. Mean strand-specific coverage profile of 3 independent experiments for Cbf11 and Cbf11DBM, and a strand-specific coverage profile for untagged WT cells (negative control) are shown. Gene orientation is indicated by three arrowheads; all three sample tracks have the same Y-axis scaling, with the maximum Y-axis value for each locus given in the top-left corner.

G) ChIP-qPCR shows the decrease in DNA binding of the Cbf11DBM-TAP protein compared to its unmutated counterpart at their selected target loci in the exponential phase. Mean ± SD values, and individual data points of 3 independent replicates are shown.

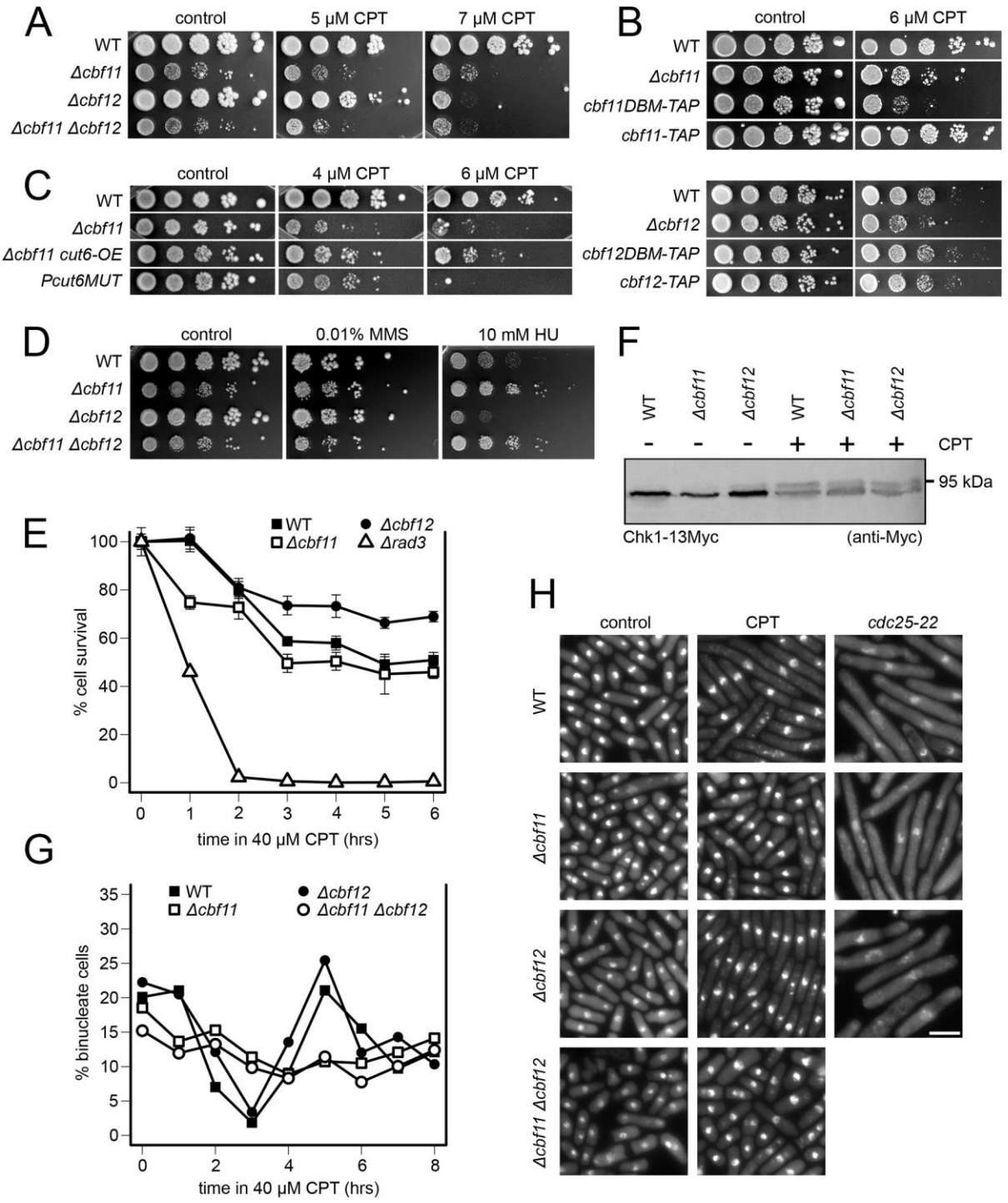

Fig. 4. CSL proteins are involved in the maintenance of genome integrity.

A-D) Cells were spotted in 10-fold serial dilutions on control and testing plates containing indicated amounts of drugs. Cell growth and survival under genotoxic stress was imaged after 2 (panel B bottom), 4 (panel C), 5 (panel A, D) or 6 (panel B top) days of incubation. Images representative of 2 independent experiments are

shown. Irrelevant parts of plate images were removed for clarity (indicated by white horizontal lines).

A) Both *Δcbf11* and *Δcbf12* cells are sensitive to camptothecin (CPT), which causes double-stranded DNA breaks, and the phenotype of the double deletion mutant is not additive.

B) Cells expressing the Cbf11DBM protein display CPT sensitivity, while cells expressing Cbf12DBM are not sensitive.

C) *Pcut6MUT* cells are also sensitive to CPT. Mild improvement of *Δcbf11* CPT sensitivity was observed upon *cut6* overexpression (*cut6-OE*).

D) Neither *Δcbf11*, nor *Δcbf12* cells display sensitivity to the genotoxic stressors methyl methanesulfonate (MMS) and hydroxyurea (HU).

E) CSL deletion mutants do not show sensitivity to acute CPT treatment, unlike the *Δrad3* DNA checkpoint kinase mutant. Cells were treated with 40 μM CPT for the indicated times, washed and the percentage of surviving cells was determined by colony formation on plates. Mean ± SD values from 3 technical replicates are shown; the whole experiment was performed twice with similar results.

F) Chk1 protein kinase is activated upon CPT-treatment in CSL deletion mutants. Western blot analysis of Chk1 activation via phosphorylation in WT, *Δcbf11*, and *Δcbf12* cells treated or not with 20 μM CPT for 2 hours in YES medium. Chk1 phosphorylation manifests as retarded migration through the gel. Image representative of 2 independent experiments is shown.

G, H) Cells lacking *cbf11* show defective cell-cycle arrest following CPT treatment. Cells were treated with 40 μM CPT for the indicated times and analyzed by microscopy. The percentage of binucleate cells was calculated (G); mean values from 2-4 independent timecourse experiments are shown. Representative images of untreated cells and cells treated with CPT for 5 hours are shown next to cells in *cdc25-22* mediated G2/M arrest (H); nuclei stained with DAPI; scale bar = 10 μm.

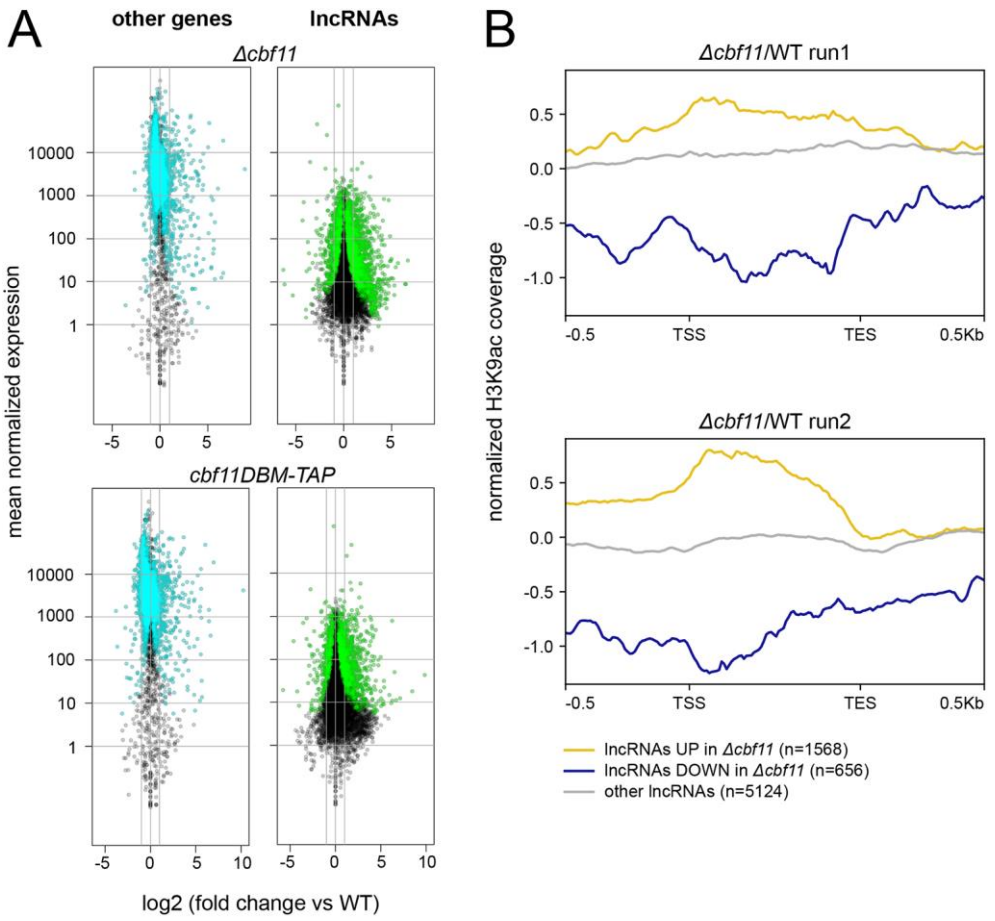

Fig. 5. Long non-coding RNAs are upregulated in both *Δcbf11* and *cbf11DBM* cells.

A) Gene expression in each mutant was determined by RNA-seq and compared to WT. For each gene, the magnitude of change in expression was plotted against its mean expression value across all samples (mutants and WT). Statistically significant differentially expressed genes are shown in cyan (other genes) or green (lncRNAs). The two gray vertical lines indicate the interval of 2-fold up- or downregulation.

B) Long ncRNA expression in the *Δcbf11* mutant correlates with H3K9 acetylation levels at the corresponding genes. Average-gene profiles of H3K9ac ChIP-seq coverage from 2 independent experiments are shown (Princová et al., 2023). TSS - transcription start site; TES - transcription end site.

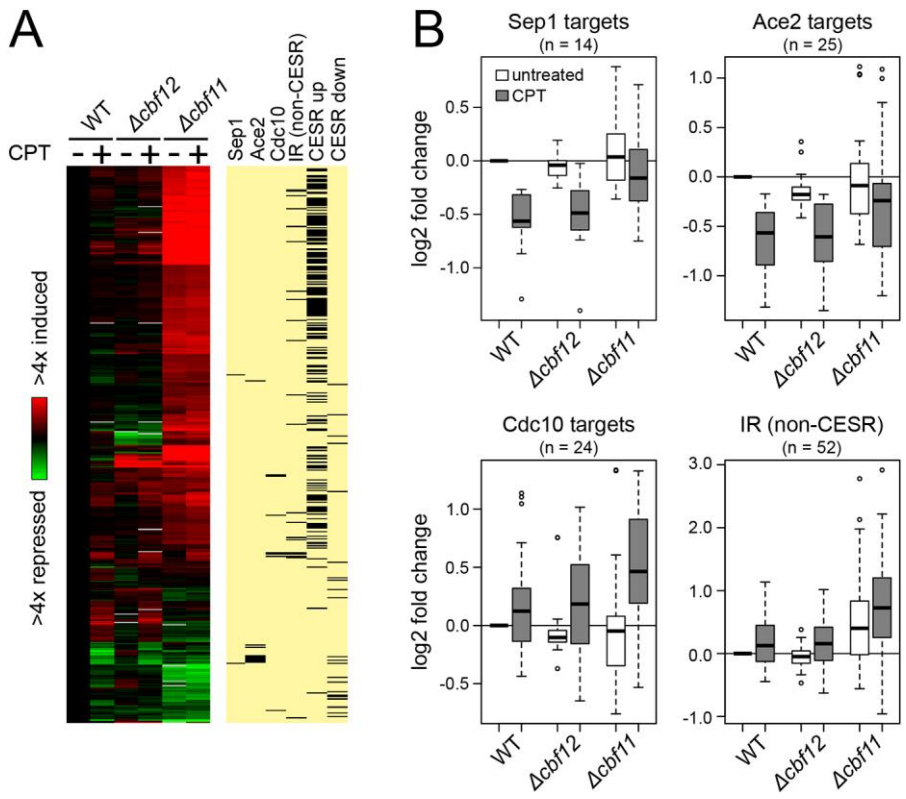

Fig. 6. Cells lacking *cbf11* show aberrant transcriptional response to CPT.
Mean values from 2 independent experiments are shown.

A) Heatmap showing gene expression changes in WT, *Δcbf12* and *Δcbf11* cells upon treatment with 20 μM CPT for 2 hours (473 genes showing at least 2-fold change in expression in at least one sample were selected). The yellow panel indicates genes regulated by Sep1, Ace2, Cdc10 (Rustici et al., 2004), induced specifically in response to ionizing radiation (IR) (Watson et al., 2004), or up- or downregulated as part of the general stress response (CESR) (Chen et al., 2003), respectively. The deregulation of CESR genes in *Δcbf11* cells was reported previously (Princová et al., 2023).

B) Distributions of expression levels of genes regulated by Sep1, Ace2, Cdc10, and induced specifically in response to IR (n indicates gene group size). Boxes show median values and 2nd and 3rd quartiles, whiskers show up to 1.5x of interquartile range, outliers are indicated as circles.

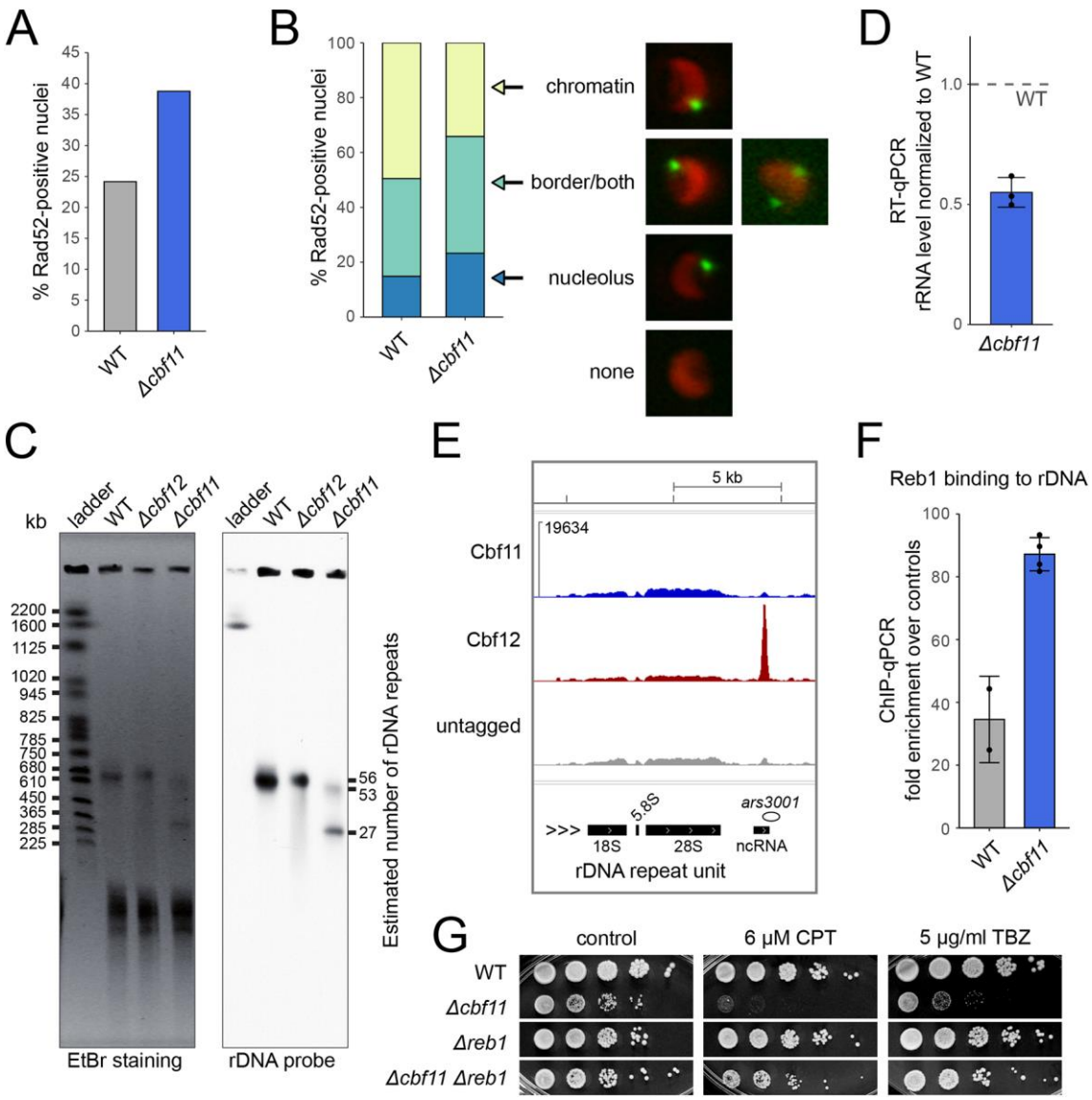

Fig. 7. Cbf11 protein is required to maintain rDNA stability

A, B) Cells lacking the *cbf11* gene show increased incidence of Rad52 DNA-repair foci, mostly in the nucleolus. Fluorescence microscopy of cells expressing proteins Hht1-mRFP (chromatin) and Rad52-YFP (DNA-repair foci) in the particular genetic background (WT or *Δcbf11*) was performed. 418 of WT nuclei and 521 of *Δcbf11* nuclei were manually evaluated for repair foci presence and subnuclear localization; representative images of cells are shown.

C) Deletion of the *cbf11* gene leads to a decrease in rDNA repeat copy number. Pulsed field gel electrophoresis with subsequent southern blot analysis probed for rDNA was performed with PvuII-digested DNA from WT, *Δcbf11*, and *Δcbf12* cells. Note that no PvuII restriction sites are present inside the rDNA arrays (Barnitz et al.,

1982). *Saccharomyces cerevisiae* chromosome DNA was used as a ladder. Images representative of 2 independent biological replicates are shown.

D) rRNA expression in WT and *Δcbf11* cells was determined by RT-qPCR. Mean ± SD values, and individual data points from 3 independent experiments are shown.

E) ChIP-seq analysis of CSL proteins revealed that Cbf12, but not Cbf11 binds to rDNA. Mean profiles of ChIP-seq coverage from two independent experiments are shown (Převorovský et al., 2015). Visualized in the Integrated Genome Viewer (IGV; Broad Institute). rDNA repeat unit (consisting of 18S, 5.8S, and 28S rDNA, and promoter and *ars3001* replication origin region) located at the right arm of chromosome 3 is depicted. All three sample tracks have the same Y-axis scaling, with the maximum Y-axis value given in the top-left corner.

F) Reb1 shows increased rDNA occupancy in *Δcbf11* cells. Mean ± SD values, and individual data points from 2 (WT) and 4 (*Δcbf11*) independent experiments are shown.

G) Deletion of *reb1* suppresses the growth defect and sensitivities to CPT and TBZ of *Δcbf11* cells. Cells were spotted in 10-fold serial dilutions on control and testing plates containing indicated amounts of drugs. Cell growth and survival was imaged after 3 days of incubation. Images representative of 2 independent experiments are shown. Irrelevant parts of plate images were removed for clarity (indicated by white horizontal lines.

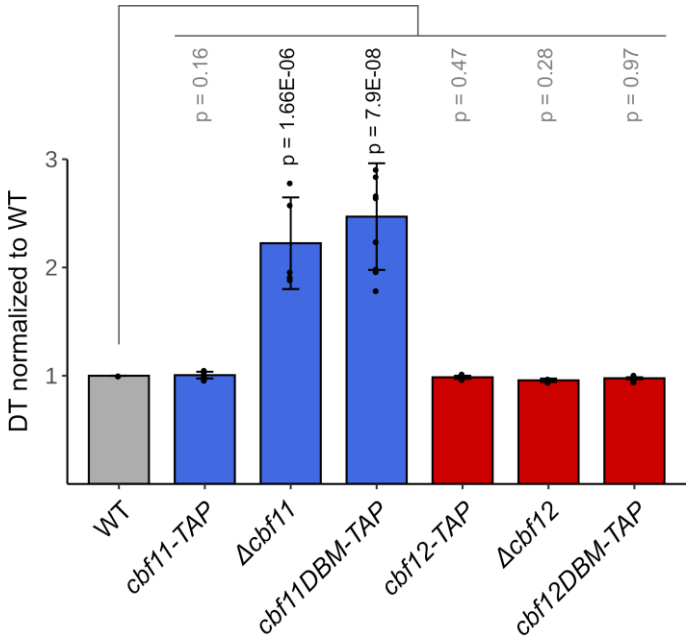

Fig. S1. The doubling times of CSL knock-outs and scarless knock-ins. The DBM mutation in Cbf11 increases the time required for biomass doubling in the same manner as *cbf11* gene deletion does. Doubling time (DT) is not affected by any genetic manipulations of the *cbf12* locus. Mean ± SD values, as well as individual data points for ≥3 independent experiments are shown. Significance was tested by a two-tailed unpaired t-test.

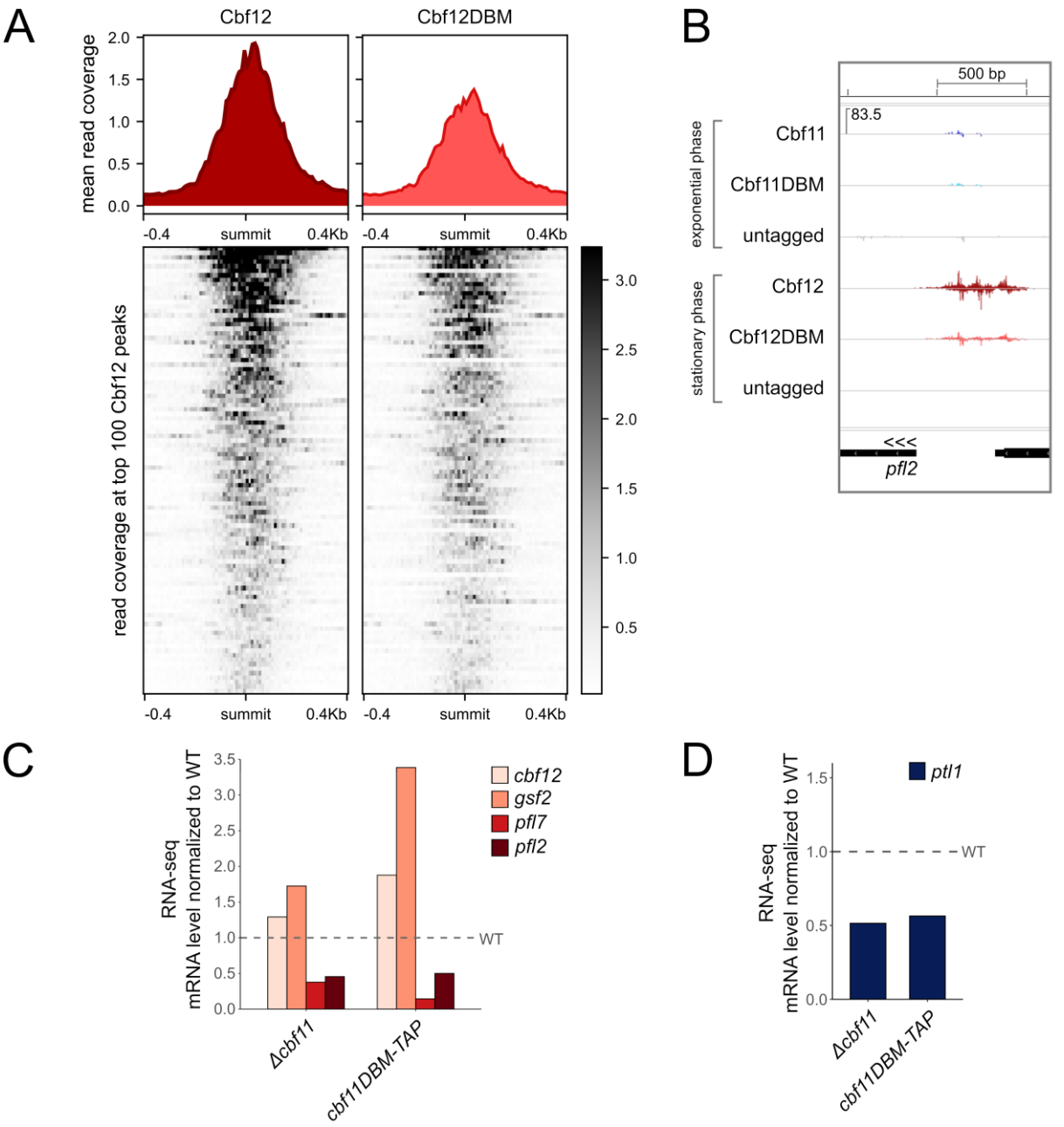

Fig. S2. ChIP-nexus and RNA-seq analyses of Cbf11 and Cbf12.

A) Compared to Cbf12, the binding of the Cbf12DBM protein to DNA is reduced genome-wide. Average-peak profiles of ChIP-nexus coverage (top) and heatmap of coverage at top 100 individual Cbf12 binding sites (bottom) are shown for Cbf12 and Cbf12DBM in the stationary phase.

B) *In vivo* binding of CSL proteins to the *pfl2* promoter was analyzed by ChIP-nexus. Mean strand-specific coverage profile of 3 independent experiments for Cbf11/12 and Cbf11DBM/12DBM, and a strand-specific coverage profile for untagged WT cells (negative control) are shown. Gene orientation is indicated by three arrowheads; all sample tracks have the same Y-axis scaling, with the maximum Y-axis value given in the top-left corner.

C, D) Expression of adhesion-related genes (C) and the lipid-related *ptl1* gene (D) in the indicated cells grown to the exponential phase determined by RNA-seq. Mean values for 3 independent experiments are shown.

E) *In vivo* binding of Cbf11 and Cbf11DBM to the promoters of additional lipid metabolism genes was analyzed by ChIP-nexus. Mean strand-specific coverage profile of 3 independent experiments for Cbf11 and Cbf11DBM, and a strand-specific coverage profile for untagged WT cells (negative control) are shown. Gene orientation is indicated by three arrowheads; all three sample tracks have the same Y-axis scaling, with the maximum Y-axis value given in the top-left corner.

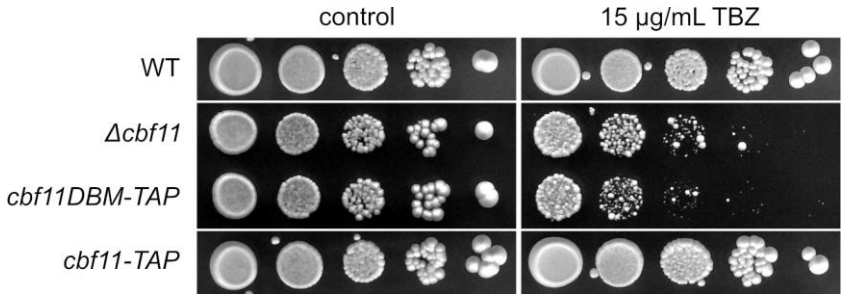

Fig. S3. Intact Cbf11 DNA-binding domain is required for resistance to microtubule poison. Both *Δcbf11* and *cbf11DBM-TAP* cells are sensitive to thiabendazole (TBZ), a microtubule-depolymerizing drug. Indicated cultures were spotted in 10-fold serial dilutions on a control plate and plate containing 15 µg/mL TBZ and were grown for 6 days. Images representative of 2 independent experiments are shown. Irrelevant parts of plate images were removed for clarity (indicated by white horizontal lines).

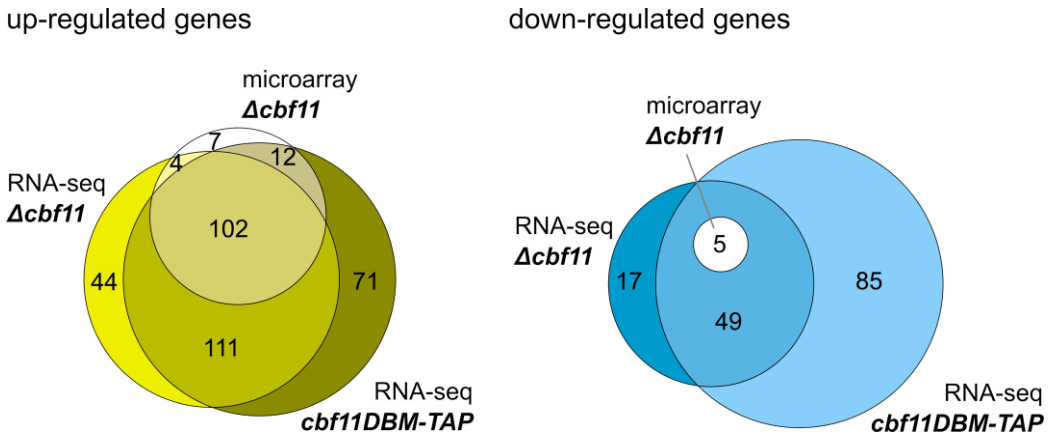

Fig. S4. Comparison of Cbf11-related RNA-seq results with previously published expression microarray data.

Venn diagram of genes showing differential expression in *Δcbf11*and *cbf11DBM-TAP* as determined by RNA-seq (this study) or microarrays (Převorovský et al., 2015). Only protein-coding genes showing at least 2-fold and statistically significant change in expression compared to WT are included.

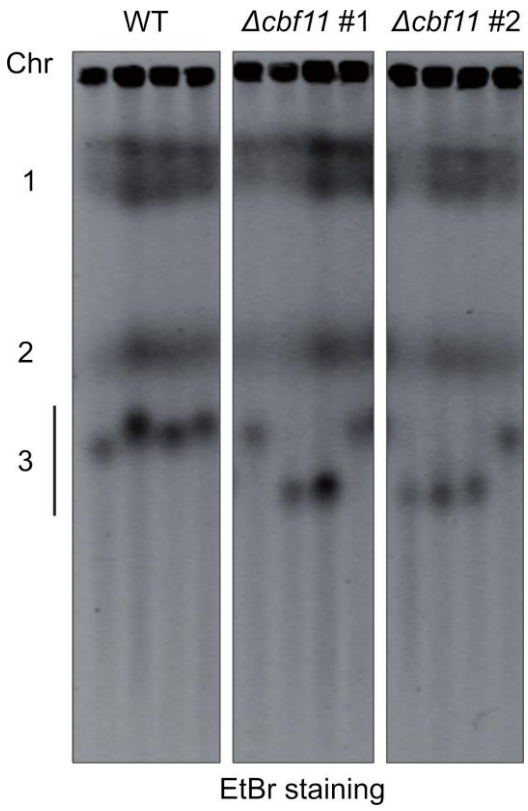

Fig. S5. The *Δcbf11* mutant displays pronounced clonal variation in the size of chromosome 3. Intact chromosomes from four WT colonies and 8 *Δcbf11* colonies obtained from two independent *Δcbf11* clones were separated by pulsed field gel electrophoresis. Image representative of 3 independent biological experiments is shown.

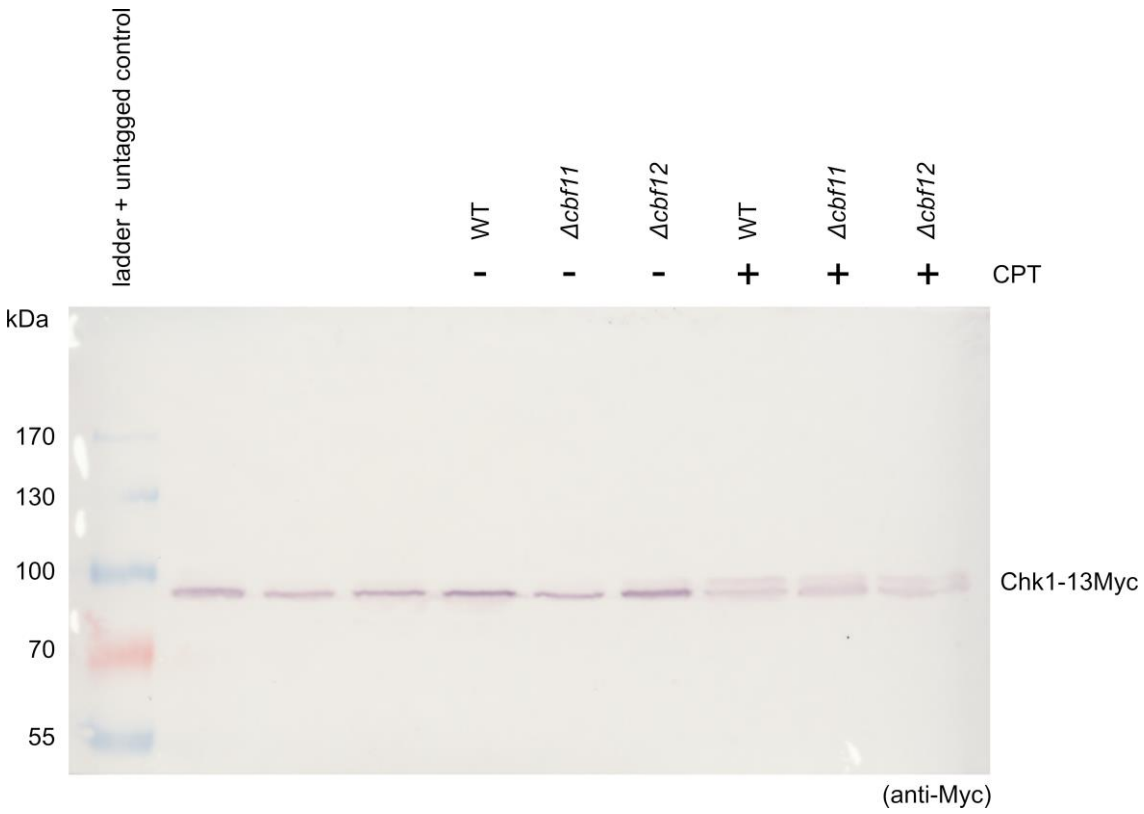

Fig. S6. Blot transparency

Full membrane corresponding to the western blot shown in Fig. 4F.

Table S1. List of strains

Available for download at
https://journals.biologists.com/jcs/article-lookup/doi/10.1242/jcs.261568#supplementary-data

Table S2. List of plasmids

Available for download at
https://journals.biologists.com/jcs/article-lookup/doi/10.1242/jcs.261568#supplementary-data

Table S3. List of primers

Available for download at
https://journals.biologists.com/jcs/article-lookup/doi/10.1242/jcs.261568#supplementary-data

Table S4. List of ChIP-nexus oligos

Available for download at
https://journals.biologists.com/jcs/article-lookup/doi/10.1242/jcs.261568#supplementary-data

Table S5.

Available for download at
https://journals.biologists.com/jcs/article-lookup/doi/10.1242/jcs.261568#supplementary-data